scientific reports

Check for updates

OPEN

High performance adaptive step size fractional numerical scheme for solving fractional differential equations

Mudassir Shams[1,2,3] & Ahmad Alalyani[4]✉

Fractional differential equations have recently gained popularity due to their ability to simulate a wide range of complex processes in various fields, including engineering, physics, biology, and finance. These equations provide a powerful framework for describing phenomena with memory effects and hereditary features that standard integer-order models cannot account for. In this study, we present fractional versions of numerical algorithms specifically designed for solving fractional-order differential equations. We thoroughly investigate the proposed approaches for stability under various fractional parameter values and compare their stability performance with existing methods. The schemes' consistency and local truncation error are calculated to ensure their accuracy. In terms of stability surface, our methods have a larger stability zone than existing fractional schemes. Two engineering applications are addressed utilizing both fixed and adaptive step-length algorithms to assess efficiency. In both cases, our methods outperform existing approaches, as evidenced by less local and global errors, reduced CPU time, and fewer function and derivative evaluations. Our newly developed fractional order technique outperforms modern high-performance algorithms in solving fractional differential equations, demonstrating superior computational efficiency and stability. These findings demonstrate the robust and efficient capabilities of the proposed methods to solve fractional-order problems.

Keywords Caputo fractional derivative, Fractional schemes, Fractional initial value problems

Abbreviations

$FEM_1^{[**]}$	Newly developed fractional IVPs
$FEM_1^{[*]} - FEM_3^{[*]}$	Fractional order schemes for solving FOIVPs
$EM^{[*]}$	Traditional Euler scheme
CPU time	Computational Time
e-	$10^{-()}$
ϑ	fractional parameter
n	Iterations

Differential equations are essential in science and engineering because they describe the relationships between changing quantities. They are significant because they enable the modeling of real-world phenomena, providing a mathematical foundation for comprehending and predicting behaviors in complex systems. In physics, they are essential for modeling motion, heat transfer, and wave propagation[1–3]. In engineering, they are fundamental for structural analysis, fluid dynamics, and control system design[4,5]. Differential equations link theory and practice, enabling engineers and scientists to design, develop, and solve global problems with precision and insight.

Fractional calculus, a generalization of traditional calculus, extends these models to systems with memory effects, making fractional-order differential equations (FODEs) indispensable for describing complex phenomena. These equations are used in fields such as control theory[6], bioengineering[7], epidemic models[8–10]

[1]Faculty of Engineering, Free University of Bozen-Bolzano, 39100 Bolzano, Italy. [2]Department of Mathematics, Faculty of Arts and Science, Balikesir University, Balikesir 10145, Turkey. [3]Department of Mathematics and Statistics, Riphah International University I-14, Islamabad 44000, Pakistan. [4]Department of Mathematics, Faculty of Science, Al-Baha University, Al-Baha 65526, Saudi Arabia. ✉email: azaher@bu.edu.sa

and financial modeling[11], where traditional models fail to capture long-term dependencies. Fractional-order initial value problems[12]:

$$\left.\begin{array}{c} D^{[\vartheta]}y(x) = f\left(x, y\left(x\right)\right), \\ y^{k}\left(\theta_0^{[*]}\right) = y_0^{k}, \end{array}\right\} \tag{1}$$

where

$$D^{[\vartheta]}y(x) = \frac{1}{\Gamma\left(m-\vartheta\right)}\int_{x_0}^{x}\frac{y^{(m)}\left(h\right)dh}{\left(x-h\right)^{\vartheta-m+1}}, m-1<\vartheta<m\in\mathbb{Z}^{+}, \tag{2}$$

$k = 0, 1, ...,\vartheta - 1$ and $x \in \left[\theta_0^{[*]}, \theta_n^{[*]}\right]$ are essential across science and engineering, modeling complex dynamics with memory effects. The complexity of fractional operators with singularities is the most significant obstacle to solving FOIVPs.

The analytical or semi-analytical techniques for solving FOIVPs —such as Laplace transforms[13,14], series expansions[15], Variation Iteration Method[16], Adomian Decomposition Method[17], Modified Homotopy Perturbation Method[18], and variable separation[19] —are often inadequate for nonlinear or high-dimensional problems due to the singularities and long-range dependencies inherent in fractional operators. Although analytical and semi-analytical methods provide exact solutions to basic problems, they are frequently ineffective for complex, nonlinear, or high-dimensional equations. These techniques require substantial symbolic integration and manipulation, limiting them unsuitable for complex settings. Extremely nonlinear situations might cause semi-analytical methods to diverge or converge slowly. Most of the time, analytical solutions yield accurate solutions; nevertheless, computing them for fractional derivatives with single kernels or memory effects is computationally expensive. In semi-analytical techniques, infinite series or approximations are often truncated, introducing errors that might spread and degrade the precision of the result.

To address these issues, several numerical methods have been devised, including the fractional Euler method[20], fractional-order Taylor's series method[21], single-step fractional-order explicit and implicit methods[22,23], and fractional Runge-Kutta methods[24]. A modification of fractional Euler method, was proposed in[25], demonstrated improved efficiency over the original method. Bhatia et al. recently offered two novel numerical modifications based on FEM and its improved version[26], together with other techniques (see, e.g.,[27,28] and references cite their in). Although these methods are helpful in solving problems, they have drawbacks including low accuracy for particularly nonlinear or unique problems, stability problems, and computational complexity. Inspired by the research mentioned above, the main aim of this study is to developed an efficient, stable and consistent fractional-order numerical schemes for solving FOIVPs.

The main contributions of this research work are as follows:

- The development of a novel one-step method for solving fractional-order initial value problems (FOIVPs) with enhanced precision and stability.
- An in-depth stability analysis is performed to ensure that the proposed approach is stable for a wide range of fractional parameters.
- Improved local truncation error estimations contribute to more accurate numerical solutions for fractional-order systems.
- A comprehensive convergence analysis illustrates that the scheme's local truncation error of 2ϑ enhances solution accuracy for fractional-order systems.
- The proposed numerical technique minimizes computational overhead, resulting in faster CPU time and memory usage when solving fractional-order initial value problems.
- The method's stability properties are tailored to ensure reliable computations even in contexts with restricted hardware capabilities or inadequate precision.

The algorithm is designed to efficiently handle large-scale FOIVPs, leveraging modern multi-core computing infrastructures. Further, most fractional techniques for solving FOIVPs used a constant step size throughout the computation, which can result in inefficiencies Such approaches may require very small steps to ensure accuracy in fast changing regions or risking significant errors if the step size is too large. In contrast, a variable step-size strategy adjusts the step size dynamically based on local error estimations. This approach enhances accuracy by refining steps in complicated regions while increasing the step size in smoother areas, hence improving computational efficiency. Additionally, it significantly improves stability control, especially for complicated issues, by preventing instability using adaptive step modifications. To overcome the limitations of fixed-step size, we incorporate a variable step-size strategy into our new fractional scheme. This incorporation automatically balances accuracy and efficiency, making our method more robust in solving FOIVPs.

The remainder of the paper is structured as follows: Section 2 introduces fundamental concepts and definitions. Section 3 provides an overview of classical and fractional-order existing numerical methods for solving FOIVPs. Section 5 the proposed fractional-order schemes , along with theoretical analyses of stability, consistency, and local truncation error. Section 6 includes numerical test problems to evaluate the efficiency and stability of the proposed method compared to existing approaches, using various benchmark stopping criteria. Finally, the conclusion is presented in the last section.

Preliminaries

Here, we discuss some basic definitions and concepts that play a major role in understanding this study. To deal with fractional-order differential equations in the sense of Caputo fractional differential, because only the Caputo derivative holds the condition of $\left[D^{[\vartheta]}\right](C) = 0$, the Riemann-Liouville integral operator of order is defined as[29]:

$$J^{[\vartheta]}\left[f\left(x\right)\right] = \frac{1}{\Gamma\left(\vartheta\right)}\int_{0}^{x}\left(\left(x-t\right)^{\vartheta-1}f(t)\right)dt, \tag{3}$$

where $x > 0, \vartheta \in (0,1], C \in \mathbb{R}$ and satisfies the following properties:

- $J^{[\vartheta_1^{[*]}]}J^{[\vartheta_2^{[*]}]}\left[f\left(x\right)\right] = J^{[\vartheta_2^{[*]}]}J^{[\vartheta_1^{[*]}]}\left[f\left(x\right)\right], \vartheta_1^{[*]}, \vartheta_2^{[*]} > 0,$
- $J^{[\vartheta_1^{[*]}]}J^{[\vartheta_2^{[*]}]}\left[f\left(x\right)\right] = J^{[\vartheta_1^{[*]}]+[\vartheta_2^{[*]}]}\left[f\left(x\right)\right], \vartheta_1^{[*]}, \vartheta_2^{[*]} > 0,$
- $J^{[\vartheta_1^{[*]}]}x^{\kappa} = \frac{\Gamma\left(\vartheta_1^{[*]}+\kappa\right)}{\Gamma\left(\vartheta_1^{[*]}+\kappa+1\right)}x^{\kappa+[\vartheta_1^{[*]}]}, \kappa > -1.$

Lemma 1 [30] *If $f \in C^n[0,b], x > 0$, and $n-1 < \vartheta \leq n$, such that $n \in \mathbb{N}$, we have*

$$D^{[\vartheta]}J^{[\vartheta]}\left[f(x)\right] = f(x), \tag{4}$$

and

$$J^{[\vartheta]}D^{[\vartheta]}\left[f(x)\right] = f(x) - \sum_{s=0}^{n-1} f^{s}\left(0^{+}\right)\frac{x^{s}}{s!}. \tag{5}$$

Lemma 2 [31] *Let $\{b_i\}_{i=0}^{s}$ be a sequance, and for any two positive real numbers v and t satisfying $b_0 \geq \frac{-t}{v}$ and $b_{i+1} \leq (1+v)\,b_i + t, \forall i = 0,1,\ldots,s$. Thus,*

$$b_{i+1} \leq \exp\left((i+1)\,v\right)\left(b_0 + \frac{t}{v}\right) - \frac{t}{v}. \tag{6}$$

Theorem 1 *Generalized Taylor's formula in the sense of the Caputo derivative about node x_0 is written as*[32]:

$$f\left(x\right) = \sum_{i=0}^{n}\frac{\left(x-x_0\right)^{i\vartheta}}{\Gamma\left(i\vartheta+1\right)}D^{[i\vartheta]}f(x_0) + \frac{\left(x-x_0\right)^{(n+1)\vartheta}}{\Gamma\left(\left(n+1\right)\vartheta+1\right)}D^{[(n+1)\vartheta]}f(\zeta), \tag{7}$$

with $0 < \zeta < x, D^{[s\vartheta]}f(x) \in C^n[0,b]$ for $s = 0,1,\ldots,n = 1, \vartheta \in (0,1]$ and $x \in (0,b]$. To further demonstrate, we can express the aforementioned formulation of the function f as follows:

$$f\left(x\right) = \begin{bmatrix} f(x_0) + \frac{(x-x_0)^{\vartheta}}{\Gamma(\vartheta+1)}D^{[\vartheta]}f(x_0) + \frac{(x-x_0)^{2\vartheta}}{\Gamma(2\vartheta+1)}D^{[2\vartheta]}f(x_0) + \ldots + \\ \frac{(x-x_0)^{i\vartheta}}{\Gamma(i\vartheta+1)}D^{[i\vartheta]}f(x_0) + \frac{(x-x_0)^{(n+1)\vartheta}}{\Gamma((n+1)\vartheta+1)}D^{[(n+1)\vartheta]}f(\zeta) \end{bmatrix}, \tag{8}$$

which can be used in the construction and analysis of the local truncation error of the fractional schemes for solving fractional-order IVPs.

Existing classical numerical schemes

Single-step techniques, such as Euler's method, the Taylor series method, and the Runge-Kutta method, are essential for solving differential equations because they are simple and adaptable. These methods are incrementally progressive, meaning that solutions are calculated at each step based on current data; consequently, they exhibit high computational efficiency. Single-step methods are especially useful for initial value problems (IVPs), as they produce highly accurate results with adaptable step sizes. Their simplicity in implementation and applicability to non-linear and time-dependent problems make them popular in engineering and scientific simulations. Furthermore, these methods serve as a foundation for advanced numerical techniques and are critical for understanding more complex algorithms.

In this section, we discuss several existing methods in the literature used to solve IVPs. The Euler method is one of the most popular methods and is given as:

$$y\left(x_{t+1}\right)=y\left(x_t\right)+hf\left(x_t,y\left(x_t\right)\right)+\left(\frac{h^2}{2!}\right)f'\left(y\left(\zeta\right)\right). \tag{9}$$

Method (9) can be approximated as:

$$\left.\begin{array}{l} g_0=y_0, \\ g_{t+1}=g_t+hf\left(x_t,g_t\right). \end{array}\right\} \tag{10}$$

The local truncation error of the Euler scheme is $O\left(h^2\right)$. Moreover, recently, the author in[33] developed the following modified version of (10) as:

$$y\left(x_{t+1}\right)=y\left(x_t\right)+hf\left(x_t+\frac{h}{2},y\left(x_t\right)+\emptyset_1^{[*]}\right)+\left(\frac{h^3}{3!}\right)f''\left(y\left(\zeta\right)\right), \tag{11}$$

where $\emptyset_1^{[*]}=\frac{h}{2}f\left(x_t,y\left(x_t\right)+\frac{h}{2}f\left(x_t,y\left(x_t\right)\right)\right)$. Method (11) can be approximated as:

$$\left.\begin{array}{l} g_0=y_0, \\ g_{t+1}=g_t+hf\left(x_t+\frac{h}{2},g_t+\frac{h}{2}f\left(x_t,g_t+\frac{h}{2}f\left(x_t,g_t\right)\right)\right). \end{array}\right\} \tag{12}$$

Method (12) can alternatively be written as:

$$\left.\begin{array}{l} g_0=y_0, \\ g_{t+1}=g_t+hk_3, \end{array}\right\} \tag{13}$$

where $k_1=f\left(x_t,g_t\right)$, $k_2=f\left(x_t,g_t+k_1\right)$, and $k_3=f\left(x_t+\frac{h}{2},g_t+k_2\right)$. The local truncation error of (13) is $O\left(h^3\right)$, and thus its order is two. Similarly, Workie[34] proposed the following scheme as:

$$y\left(x_{t+1}\right)=y\left(x_t\right)+hf\left(x_t+\frac{h}{2},y\left(x_t\right)+\frac{h}{2}\emptyset_2^{[*]}\right)+\left(\frac{h^3}{3!}\right)f''\left(y\left(\zeta\right)\right), \tag{14}$$

where $\emptyset_2^{[*]}=f\left(x_t,y\left(x_t\right)+\frac{h}{2}f\left(x_t,y\left(x_t\right)+hf(x_t,y\left(x_t\right)+hf\left(x_t,y\left(x_t\right)\right)\right)\right)\right)$. Method (14) can be approximated as:

$$\left.\begin{array}{l} g_0=y_0, \\ g_{t+1}=g_t+hf\left(x_t+\frac{h}{2},g_t+\frac{h}{2}f\left(x_t,\emptyset_3^{[*]}\right)\right), \end{array}\right\} \tag{15}$$

where $\emptyset_3^{[*]}=g_t+\frac{h}{2}f\left(x_t,g_t+hf((x_t,g_t+hf\left(x_t,g_t\right)\right)))$. Method (15) can alternatively be written as:

$$\left.\begin{array}{l} g_0=y_0, \\ g_{t+1}=g_t+hk_4, \end{array}\right\} \tag{16}$$

where $k_1=f\left(x_t,g_t\right)$, $k_2=f\left(x_t,g_t+hk_1\right)$, $k_3=f\left(x_t,g_t+\frac{h}{2}k_2\right)$, and $k_4=f\left(x_t,g_t+\frac{h}{2}k_3\right)$. The local truncation error of (16) is $O\left(h^3\right)$, and thus its order is two. Using harmonic mean, Workie[35] provides the following scheme:

$$y\left(x_{t+1}\right)=y\left(x_t\right)+h\frac{\left[\left(f\left(x_t,y\left(x_t\right)\right)\right)^2+\left(f\left(x_t+h,\emptyset_4^{[*]}\right)\right)^2\right]}{\left[f\left(x_t,y\left(x_t\right)\right)+f\left(x_t+h,\emptyset_4^{[*]}\right)\right]}+\left(\frac{h^3}{3!}\right)f''\left(y\left(\zeta\right)\right), \tag{17}$$

where $\emptyset_4^{[*]}=y\left(x_t\right)+hf\left(x_t,y\left(x_t\right)\right)$. Method (17) can be approximated as:

$$\left.\begin{array}{l} g_0=y_0, \\ g_{t+1}=g_t+h\frac{\left(f\left(x_t,g_t\right)\right)^2+\left(f\left(x_t+h,g_t+hf\left(x_t,g_t\right)\right)\right)^2}{f\left(x_t,g_t\right)+f\left(x_t+h,g_t+hf\left(x_t,g_t\right)\right)} \end{array}\right\}. \tag{18}$$

Method (18) can alternatively be written as:

$$\left.\begin{array}{l} g_0=y_0, \\ g_{t+1}=g_t+h\frac{(k_1)^2+(k_2)^2}{k_1+k_2}, \end{array}\right\} \tag{19}$$

where $k_1=f\left(x_t,g_t\right)$ and $k_2=f\left(x_t,g_t+hk_1\right)$. The local truncation error of the (18) is $O\left(h^3\right)$, and thus its order is two.

Construction and analysis of modified fractional schemes

To solve fractional differential equations (FDEs), conventional fractional-order numerical methods—such as Grünwald-Letnikov and Caputo-based schemes—are essential because they capture the memory and inheritance effects that are inherent to fractional systems. The inherent memory and genetic effects in such systems necessitate more sophisticated models than those that describe typical long-term dependencies, frequently providing an advantage in handling ordinary differential equations. Fractional methods are more adaptable for simulating complex, real-world phenomena such as anomalous diffusion and viscoelasticity. They effectively capture dynamics that traditional ODE approaches miss, particularly in systems with power-law behavior. These methods offer deeper insights into processes with fractional dynamics, thereby more accurately depicting the intricacies of nature.

In this section, we discuss several existing methods in the literature used to solve initial value problems (IVPs). The Euler method is given as:

$$y\left(x_{t+1}\right)=y\left(x_t\right)+\left(\frac{h^{\vartheta}}{\Gamma\left(\vartheta+1\right)}\right)f\left(x_t,y\left(x_t\right)\right)+\left(\frac{h^2}{2!}\right)D^{[2\vartheta]}\left(y\left(\zeta\right)\right). \tag{20}$$

Method (20) can be approximated as:

$$\left.\begin{aligned} g_0&=y_0,\\ g_{t+1}&=g_t+\tfrac{h^{\vartheta}}{\Gamma(\vartheta+1)}f\left(x_t,g_t\right). \end{aligned}\right\} \tag{21}$$

The local truncation error of the Euler scheme is $O\left(\frac{h^{2\vartheta}}{\Gamma(2\vartheta+1)}\right)$. The fractional version of the scheme (12) is provided as[36]:

$$y\left(x_{t+1}\right)=y\left(x_t\right)+\frac{h^{\vartheta}}{\Gamma\left(\vartheta+1\right)}f\left(x_t+\frac{h^{\vartheta}}{2\Gamma\left(\vartheta+1\right)},y\left(x_t\right)+\wp\right)+O\left(\frac{h^{3\vartheta}}{\Gamma\left(3\vartheta+1\right)}\right)D^{[3\vartheta]}\left(y\left(\zeta\right)\right), \tag{22}$$

where $\wp=\frac{h^{\vartheta}}{2\Gamma(\vartheta+1)}f\left(x_t,y\left(x_t\right)+\frac{h^{\vartheta}}{2\Gamma(\vartheta+1)}f\left(x_t,y\left(x_t\right)\right)\right)$. Method (22) can be approximated as:

$$\left.\begin{aligned} &g_0=y_0,\\ &g_{t+1}=g_t+\tfrac{h^{\vartheta}}{\Gamma(\vartheta+1)}f\left(x_t+\left(\tfrac{1}{2}\tfrac{h^{\vartheta}}{\Gamma(\vartheta+1)}\right),g_t+\left(\tfrac{1}{2}\tfrac{h^{\vartheta}}{\Gamma(\vartheta+1)}\right)f\left(x_t,g_t+\left(\tfrac{1}{2}\tfrac{h^{\vartheta}}{\Gamma(\vartheta+1)}\right)f\left(x_t,g_t\right)\right)\right). \end{aligned}\right\} \tag{23}$$

Method (23) can alternatively be written as:

$$\left.\begin{aligned} g_0&=y_0,\\ g_{t+1}&=g_t+\tfrac{h^{\vartheta}}{\Gamma(\vartheta+1)}k_3, \end{aligned}\right\} \tag{24}$$

where $k_1=f\left(x_t,g_t\right)$, $k_2=f\left(x_t,g_t+k_1\right)$, and $k_3=f\left(x_t+\left(\frac{1}{2}\frac{h^{\vartheta}}{\Gamma(\vartheta+1)}\right),g_t+\left(\frac{1}{2}\frac{h^{\vartheta}}{\Gamma(\vartheta+1)}\right)k_2\right)$. The fractional order scheme (24) is abbreviated as $\mathrm{FEM}_1^{[*]}$[37]. The local truncation error of the fractional scheme (24) is as follows:

$$y\left(x_{t+1}\right)-g_{t+1}\approx\wp_1^{[*]}\left(\frac{h^{3\vartheta}}{\Gamma\left(3\vartheta+1\right)}\right)+O\left(\frac{h^{4\vartheta}}{\Gamma\left(4\vartheta+1\right)}\right)D^{[3\vartheta]}\left(y\left(\zeta\right)\right), \tag{25}$$

where $\wp_1^{[*]}=\left(\frac{1}{24}D_{xx}^{[\vartheta]}f+\frac{1}{6}D_x^{[\vartheta]}fD_y^{[\vartheta]}f+\frac{1}{24}{}_x^{[\vartheta]}f^2D_{yy}^{[\vartheta]}f+\frac{1}{12}fD_{xy}^{[\vartheta]}f-\frac{1}{12}f\left(D_y^{[\vartheta]}f\right)^2\right)$. Thus, the fractional scheme is of order 2ϑ with a local truncation error of $O\left(\frac{h^{3\vartheta}}{\Gamma(3\vartheta+1)}\right)D^{[3\vartheta]}\left(y\left(\zeta\right)\right)$. The fractional scheme (25) is consistent and stable according to Dahlquist's test[38], and the related stability function is given as:

$$Q\left(z\right)=\left(\frac{g_{t+1}}{g_t}\right)=1+z+\frac{1}{2}z^2+\frac{1}{4}z^3. \tag{26}$$

where $z=\frac{\hat{h}}{\Gamma(\vartheta+1)}$ and $\hat{h}=h^{\vartheta}\lambda$. Similarly, Batiha et al.[26] proposed the following scheme as:

$$y\left(x_{t+1}\right)=y\left(x_t\right)+\frac{h^{\vartheta}}{\Gamma\left(\vartheta+1\right)}f\left(x_t+\left(\frac{h^{\vartheta}}{\Gamma\left(\vartheta+1\right)}\right),y\left(x_t\right)+\left(\frac{h^{\vartheta}}{\Gamma\left(\vartheta+1\right)}\right)f\left(x_t,y\left(x_t\right)+y^*\right)\right)+O\left(\frac{h^{3\vartheta}}{\Gamma\left(3\vartheta+1\right)}\right)D^{[3\vartheta]}\left(y\left(\zeta\right)\right), \tag{27}$$

where

$$y^{*}=\left(\frac{h^{\vartheta}}{2\Gamma\left(\vartheta+1\right)}\right)f\left(x_{t},y\left(x_{t}\right)+\frac{h^{\vartheta}}{\Gamma\left(\vartheta+1\right)}f(x_{t},y\left(x_{t}\right)\right). \tag{28}$$

Method (27) can be approximated as:

$$\left.\begin{array}{l} g_{0}=y_{0},\\ g_{t+1}=g_{t}+\frac{h^{\vartheta}}{\Gamma(\vartheta+1)}f'\left(x_{t}+\frac{h^{\vartheta}}{\Gamma(\vartheta+1)},g_{t}+\frac{h^{\vartheta}}{\Gamma(\vartheta+1)}f\left(x_{t},\wp_{2}^{[*]}\right)\right), \end{array}\right\} \tag{29}$$

where $\wp_{2}^{[*]}=g_{t}+\frac{h^{\vartheta}}{\Gamma(\vartheta+1)}f\left(x_{t},g_{t}+\frac{h^{\vartheta}}{\Gamma(\vartheta+1)}f\left(x_{t},g_{t}\right)\right)$. The fractional order scheme (29) is abbreviated as $\mathrm{FEM}_{2}^{[*]}$. Method (29) can alternatively be written as:

$$\left.\begin{array}{l} g_{0}=y_{0},\\ g_{t+1}=g_{t}+\frac{h^{\vartheta}}{\Gamma(\vartheta+1)}k_{3}, \end{array}\right\} \tag{30}$$

where $k_{1}=f\left(x_{t},g_{t}\right)$, $k_{2}=f\left(x_{t},g_{t}+\frac{h^{\vartheta}}{2\Gamma(\vartheta+1)}k_{1}\right)$, and $k_{3}=f\left(x_{t},g_{t}+\left(\frac{h^{\vartheta}}{2\Gamma(\vartheta+1)}\right)k_{2}\right)$. The local truncation error of the fractional scheme (30) is as follows:

$$y\left(x_{t+1}\right)-g_{t+1}\approx\wp_{3}^{[*]}\left(\frac{h^{2\vartheta}}{\Gamma\left(2\vartheta+1\right)}\right)+O\left(\frac{h^{3\vartheta}}{\Gamma\left(3\vartheta+1\right)}\right)D^{[3\vartheta]}\left(y\left(\zeta\right)\right), \tag{31}$$

where $\wp_{3}^{[*]}=\left(\frac{1}{12}fD_{xy}^{[\vartheta]}f+\frac{1}{2}f^{2}D_{yy}^{[\vartheta]}f+\frac{1}{6}D_{x}^{[\vartheta]}fD_{y}^{[\vartheta]}f-\frac{1}{24}D_{xx}^{[\vartheta]}f-\frac{1}{3}f\left(D_{y}^{[\vartheta]}f\right)^{2}\right)$. Thus, the fractional scheme (31) is of order 2ϑ with a local truncation error of $O\left(\frac{h^{3\vartheta}}{\Gamma(3\vartheta+1)}\right)D^{[3\vartheta]}\left(y\left(\zeta\right)\right)$. The fractional scheme (31) is consistent and stable, and the associated stability function is given as:

$$Q\left(z\right)=1+z+\frac{1}{2}\left(z^{2}+z^{3}+z^{4}\right), \tag{32}$$

where $z=\frac{\hat{h}}{\Gamma(\vartheta+1)}$ and $\hat{h}=h^{\vartheta}\lambda$. The fractional version of (17) is given as:

$$\begin{aligned} y\left(x_{t+1}\right)=&y\left(x_{t}\right)+\frac{h^{\vartheta}}{\Gamma\left(\vartheta+1\right)}\frac{\left[\left(f\left(x_{t},y\left(x_{t}\right)\right)\right)^{2}+\left(f\left(x_{t}+\left(\frac{h^{\vartheta}}{\Gamma(\vartheta+1)}\right),\wp_{4}^{[*]}\right)\right)^{2}\right]}{\left[f\left(x_{t},y\left(x_{t}\right)\right)+f\left(x_{t}+\left(\frac{h^{\vartheta}}{\Gamma(\vartheta+1)}\right),\wp_{5}^{[*]}\right)\right]}\\ &+\left(\frac{h^{3\vartheta}}{\Gamma\left(3\vartheta+1\right)}\right)D^{[3\vartheta]}\left(y\left(\zeta\right)\right), \end{aligned} \tag{33}$$

where $\wp_{4}^{[*]}=y\left(x_{t}\right)+\left(\frac{h^{\vartheta}}{\Gamma(\vartheta+1)}\right)f\left(x_{t},\,y\left(x_{t}\right)\right)$, $\wp_{5}^{[*]}=y\left(x_{t}\right)+\left(\frac{h^{\vartheta}}{\Gamma(\vartheta+1)}\right)f\left(x_{t},y\left(x_{t}\right)\right)$. Method (33) can be approximated as:

$$\left.\begin{array}{l} g_{0}=y_{0},\\ g_{t+1}=g_{t}+\frac{h^{\vartheta}}{\Gamma(\vartheta+1)}\left(\frac{(f(x_{t},g_{t}))^{2}+\left(f\left(x_{t}+\frac{h^{\vartheta}}{\Gamma(\vartheta+1)},g_{t}+\frac{h^{\vartheta}}{\Gamma(\vartheta+1)}f(x_{t},g_{t})\right)\right)^{2}}{f(x_{t},g_{t})+f\left(x_{t}+\frac{h^{\vartheta}}{\Gamma(\vartheta+1)},g_{t}+\frac{h^{\vartheta}}{\Gamma(\vartheta+1)}f(x_{t},g_{t})\right)}\right). \end{array}\right\} \tag{34}$$

Method (34) can alternatively be written as:

$$\left.\begin{array}{l} g_{0}=y_{0},\\ g_{t+1}=g_{t}+\frac{h^{\vartheta}}{\Gamma(\vartheta+1)}\frac{(k_{1})^{2}+(k_{2})^{2}}{k_{1}+k_{2}}, \end{array}\right\} \tag{35}$$

where $k_{1}=f\left(x_{t},g_{t}\right)$ and $k_{2}=f\left(x_{t},g_{t}+\frac{h^{\vartheta}}{\Gamma(\vartheta+1)}k_{1}\right)$. The fractional order scheme (35) is abbreviated as $\mathrm{FEM}_{3}^{[*]}$. The local truncation error of the fractional scheme is given as:

$$y\left(x_{t+1}\right)-g_{t+1}\approx\wp_{6}^{[*]}\left(\frac{h^{2\vartheta}}{\Gamma\left(2\vartheta+1\right)}\right)+O\left(\frac{h^{3\vartheta}}{\Gamma\left(3\vartheta+1\right)}\right)D^{[3\vartheta]}\left(y\left(\zeta\right)\right), \tag{36}$$

where $\wp_6^{[*]} = \left(\frac{1}{6} f D_{xy}^{[\vartheta]} f - \frac{1}{12} f^2 D_{yy}^{[\vartheta]} f - \frac{1}{3} D_x^{[\vartheta]} f D_y^{[\vartheta]} f - \frac{1}{4} \frac{\left(D_{xy}^{[\vartheta]} f\right)^2}{f} - \frac{1}{12} f \left(D_y^{[\vartheta]} f\right)^2\right)$. Thus, the fractional scheme (36) is of order 2ϑ with a local truncation error of $O\left(\frac{h^{3\vartheta}}{\Gamma(3\vartheta+1)}\right) D^{[3\vartheta]}(y(\zeta))$. The fractional scheme (36) is consistent and stable, and the associated stability function is given as:

$$Q(z) = 1 + \left(\frac{z^2 + \left(z + z^2\right)^2}{2z + z^2}\right), \tag{37}$$

where $z = \frac{\hat{h}}{\Gamma(\vartheta+1)}$ and $\hat{h} = h^{\vartheta}\lambda$.

Development of fractional schemes and their consistency and stability analysis

In this subsection, we present the following fractional version of the technique to solve IVPs in classical calculus, as explored and proposed in[39]:

$$\begin{aligned} y(x_{t+1}) = y(x_t) + \frac{h^{\vartheta}}{\Gamma(\vartheta+1)} \frac{\left[\begin{array}{c} (f(x_t, y(x_t)))^2 + \\ \left(f\left(x_t + \left(\frac{h^{\vartheta}}{\Gamma(\vartheta+1)}\right), y(x_t) + \left(\frac{h^{\vartheta}}{\Gamma(\vartheta+1)}\right) y^{**}\right)\right)^2 \end{array}\right]}{\left[\begin{array}{c} f(x_t, y(x_t)) + \\ f\left(x_t + \left(\frac{h^{\vartheta}}{\Gamma(\vartheta+1)}\right), y(x_t) + \left(\frac{h^{\vartheta}}{\Gamma(\vartheta+1)}\right) y^{**}\right) \end{array}\right]} \\ + \left(\frac{h^{3\vartheta}}{\Gamma(3\vartheta+1)}\right) D^{[3\vartheta]}(y(\zeta)), \end{aligned} \tag{38}$$

where $y^{**} = \left(\frac{f(x_t, y(x_t)) + f\left(x_t + \left(\frac{h^{\vartheta}}{\Gamma(\vartheta+1)}\right), y(x_t) + \left(\frac{h^{\vartheta}}{\Gamma(\vartheta+1)}\right) f(x_t, y(x_t))\right)}{2}\right)$. Method (38) can be approximated as:

$$\left.\begin{array}{l} g_0 = y_0, \\ g_{t+1} = g_t + \frac{h^{\vartheta}}{\Gamma(\vartheta+1)} \frac{(f(x_t, g_t))^2 + \left(f\left(x_t + \left(\frac{h^{\vartheta}}{\Gamma(\vartheta+1)}\right), g_t + \left(\frac{h^{\vartheta}}{\Gamma(\vartheta+1)}\right) y_1^{**}\right)\right)^2}{f(x_t, g_t) + f\left(x_t + \left(\frac{h^{\vartheta}}{\Gamma(\vartheta+1)}\right), g_t + \left(\frac{h^{\vartheta}}{\Gamma(\vartheta+1)}\right) y_1^{**}\right)}, \end{array}\right\} \tag{39}$$

where $y_1^{**} = \left(\frac{f(x_t, g_t) + f\left(x_t + \left(\frac{h^{\vartheta}}{\Gamma(\vartheta+1)}\right), g_t + \left(\frac{h^{\vartheta}}{\Gamma(\vartheta+1)}\right) f(x_t, g_t)\right)}{2}\right)$. Method (39) can alternatively be written as:

$$\left.\begin{array}{l} g_0 = y_0, \\ g_{t+1} = g_t + \frac{h^{\vartheta}}{\Gamma(\vartheta+1)} \frac{(k_1)^2 + (k_3)^2}{k_1 + k_3}, \end{array}\right\} \tag{40}$$

where $k_1 = f(x_t, g_t)$, $k_2 = f\left(x_t + \frac{h^{\vartheta}}{\Gamma(\vartheta+1)}, g_t + \frac{h^{\vartheta}}{\Gamma(\vartheta+1)} k_1\right)$, $k_3 = f\left(x_t + \frac{h^{\vartheta}}{\Gamma(\vartheta+1)}, g_t + \frac{h^{\vartheta}}{\Gamma(\vartheta+1)} \left(\frac{k_1+k_2}{2}\right)\right)$. The fractional order scheme (40) is abbreviated as $\mathrm{FEM}_1^{[**]}$.

Accuracy of the proposed fractional scheme

The local truncation error are essential for solving IVP using numerical schemes because it indicates computational dependability by analyzing the solution's accuracy at each step. This understanding and minimization keep the numerical approach stable and convergent. This local truncation error can be well controlled to yield better approximations for many sensitive or highly nonlinear situations. Using Taylor's series expansion of $y(x_{t+1})$ for the highest possible term, we get:

$$y(x_{t+1}) = y(x_t) + \frac{h^{\vartheta}}{\Gamma(\vartheta+1)} D^{[\vartheta]} y(x_t) + \frac{h^{2\vartheta}}{\Gamma(2\vartheta+1)} D^{[2\vartheta]} y(x_t) + \frac{h^{3\vartheta}}{\Gamma(3\vartheta+1)} D^{[3\vartheta]} y(x_t) + \cdots \tag{41}$$

Equation (41) yields the following when we express the derivatives of *y* in terms of *f*:

$$y(x_{t+1}) = y(x_t) + \frac{h^{\vartheta}}{\Gamma(\vartheta+1)} f + \frac{h^{2\vartheta}}{\Gamma(2\vartheta+1)} \left(D_x^{[\vartheta]} f + f D_y^{[\vartheta]} f\right) + \ldots \tag{42}$$

where $f = f(x, y(x))$ is used for simplification. Simillarly, using Taylor's series expansion of k_1, k_2, and k_3 and (40) yields the following:

$$k_1 = f, \tag{43}$$

$$k_2 = \frac{h^{\vartheta}}{\Gamma(\vartheta+1)} f + \left(D_x^{[\vartheta]} f + f D_y^{[\vartheta]} f\right) \frac{h^{2\vartheta}}{\Gamma(2\vartheta+1)} + \frac{1}{2}\left(f^2 D_{yy}^{[\vartheta]} f + f D_{xy}^{[\vartheta]} f + \frac{1}{2} D_{xx}^{[\vartheta]} f\right) \frac{h^{3\vartheta}}{\Gamma(3\vartheta+1)} + \ldots \tag{44}$$

Taking the average of (43) and (44), we yield:

$$\frac{k_1+k_2}{2} = \frac{h^{\vartheta}}{\Gamma(\vartheta+1)} f + \left(\frac{1}{2} D_x^{[\vartheta]} f + \frac{1}{2} f D_y^{[\vartheta]} f\right) \frac{h^{2\vartheta}}{\Gamma(2\vartheta+1)} + \left(\frac{1}{4} D_{xx}^{[\vartheta]} f + \frac{1}{2} f D_{xy}^{[\vartheta]} f + \frac{1}{4} f^2 D_{yy}^{[\vartheta]} f + \frac{1}{4} f \left(D_y^{[\vartheta]} f\right)^2 + \frac{1}{4} D_x^{[\vartheta]} f D_y^{[\vartheta]} f\right) \frac{h^{3\vartheta}}{\Gamma(3\vartheta+1)} + \ldots \tag{45}$$

$$k_3 = \frac{h^{\vartheta}}{\Gamma(\vartheta+1)} f^2 + 2f \left(D_x^{[\vartheta]} f + f D_y^{[\vartheta]} f\right) \frac{h^{2\vartheta}}{\Gamma(2\vartheta+1)} + \left(2f\left(\frac{1}{2} D_{xx}^{[\vartheta]} f + f D_{xy}^{[\vartheta]} f + \frac{1}{2} f^2 D_{yy}^{[\vartheta]} f + \frac{1}{2} f \left(D_y^{[\vartheta]} f\right)^2 + \frac{1}{2} D_x^{[\vartheta]} f D_y^{[\vartheta]} f\right)\right) \frac{h^{3\vartheta}}{\Gamma(3\vartheta+1)} + \ldots \tag{46}$$

By taking the square of (43) and (46) and then adding, we get the following expression:

$$k_1^2 + k_3^2 = \frac{2h^{\vartheta}}{\Gamma(\vartheta+1)} f^2 + 2f \left(D_x^{[\vartheta]} f + f D_y^{[\vartheta]} f\right) \frac{h^{2\vartheta}}{\Gamma(2\vartheta+1)} + \left(2f\left(\begin{array}{c} \frac{1}{2} D_{xx}^{[\vartheta]} f + f D_{xy}^{[\vartheta]} f + \frac{1}{2} f^2 D_{yy}^{[\vartheta]} f + \frac{1}{2} f \left(D_y^{[\vartheta]} f\right)^2 \\ + \frac{1}{2} D_x^{[\vartheta]} f D_y^{[\vartheta]} f + \left(D_x^{[\vartheta]} f + f D_y^{[\vartheta]} f\right)^2 \end{array}\right)\right) \frac{h^{3\vartheta}}{\Gamma(3\vartheta+1)} + \ldots \tag{47}$$

Adding (43) and (44) and then taking its inverse yields the following:

$$(k_1+k_3)^{-1} = \frac{\frac{h^{\vartheta}}{\Gamma(\vartheta+1)}}{2f} - \frac{\frac{h^{2\vartheta}}{\Gamma(2\vartheta+1)}}{4}\left(\frac{\left(D_x^{[\vartheta]} f + f D_y^{[\vartheta]} f\right)}{f^2}\right) + \frac{1}{2f}\left(-\frac{D_1^{[*]}}{2f} + \frac{\frac{h^{2\vartheta}}{\Gamma(2\vartheta+1)}}{4}\left(\frac{\left(D_x^{[\vartheta]} f + f D_y^{[\vartheta]} f\right)^2}{f^2}\right)\right) \frac{h^{3\vartheta}}{\Gamma(3\vartheta+1)} + \ldots \tag{48}$$

where $D_1^{[*]} = \frac{1}{2} D_{xx}^{[\vartheta]} f + f D_{xy}^{[\vartheta]} f + \frac{1}{2} f^2 D_{yy}^{[\vartheta]} f + \frac{1}{2} f \left(D_y^{[\vartheta]} f\right)^2 + \frac{1}{2} D_x^{[\vartheta]} f D_y^{[\vartheta]} f$. Substituting (47) and (48) into (40), we have:

$$g_{t+1} = g_t + \frac{h^{\vartheta}}{\Gamma(\vartheta+1)} f + \left(\frac{1}{2} D_x^{[\vartheta]} f + \frac{1}{2} f D_y^{[\vartheta]} f\right) \frac{h^{2\vartheta}}{\Gamma(2\vartheta+1)} + \ldots \tag{49}$$

Subtracting Eq. (49) from Eq. (42) yields the local truncation error (LTE) as:

$$LTE = \left(-\frac{1}{12} D_{xx}^{[\vartheta]} f - D_2^{[*]} - \frac{1}{4} \frac{\left(D_x^{[\vartheta]} f\right)^2}{f} - \frac{1}{6} f D_{xy}^{[\vartheta]} f\right) \frac{h^{3\vartheta}}{\Gamma(3\vartheta+1)} D^{[3\vartheta]}\left(y(\zeta)\right), \tag{50}$$

where $D_2^{[*]} = \frac{1}{12} f^2 D_{yy}^{[\vartheta]} f - \frac{1}{3} f \left(D_y^{[\vartheta]} f\right)^2 - \frac{7}{12} D_x^{[\vartheta]} f D_y^{[\vartheta]} f$. Thus, the fractional scheme is of order 2ϑ with a local truncation error of $O\left(\frac{h^{3\vartheta}}{\Gamma(3\vartheta+1)}\right) D^{[3\vartheta]}\left(y(\zeta)\right)$.

Consistency analysis of the fractional scheme

If a numerical method is consistent, the discretized equations will eventually converge to the exact differential equation solutions as the step size approaches zero. Using consistent numerical techniques is essential to obtaining accurate and reliable outcomes. The consistency of the scheme (40) is computed as follows:

$$g_{t+1} = g_t + \frac{h^{\vartheta}}{\Gamma(\vartheta+1)} \Phi(x_t, g_t, h), \tag{51}$$

if $\lim_{h\to 0}\Phi\left(x_t, g_t, h\right) = f\left(x_t, g_t\right)$, therefore

$$\lim_{h\to 0}\Phi\left(x_t, g_t, h\right) = \lim_{h\to 0}\left(\frac{\left(f\left(x_t, g_t\right)\right)^2 + \left(f\left(x_t + \frac{h^{\vartheta}}{\Gamma(\vartheta+1)}, g_t + \frac{h^{\vartheta}}{\Gamma(\vartheta+1)}\frac{k_1+k_2}{2}\right)\right)^2}{f\left(x_t, g_t\right) + f\left(x_t + \frac{h^{\vartheta}}{\Gamma(\vartheta+1)}, g_t + \frac{h^{\vartheta}}{\Gamma(\vartheta+1)}\frac{k_1+k_2}{2}\right)}\right), \tag{52}$$

$$= \frac{2\left(f\left(x_t, g_t\right)\right)^2}{2f\left(x_t, g_t\right)} = f\left(x_t, g_t\right), \tag{53}$$

where $k_1 = f\left(x_t, g_t\right)$ and $k_2 = f\left(x_t + \frac{h^{\vartheta}}{\Gamma(\vartheta+1)}, g_t + \frac{h^{\vartheta}}{\Gamma(\vartheta+1)}k_1\right)$.

Stability analysis of the fractional scheme

Errors should not increase uncontrollably as computations advance, particularly for complex or highly sensitive problems. A stable approach ensures that slight changes in the initial conditions and at each step do not result in major deviations in the solution. The stability region of a numerical scheme refers to the range of step sizes and problem parameters for which the approach is stable. This knowledge is crucial for selecting appropriate methods for solving IVPs for different types of problems. Stability analysis is important in ensuring reliable and accurate results in long-term simulations or complex systems. The Dahlquist's test problem is used to calculate the stability of the suggested fractional scheme (40) as follows:

$$\left.\begin{array}{c} D^{[\vartheta]}g\left(x\right) = \lambda g\left(x\right); \lambda \in \mathbb{C}; 0 < \vartheta < 1, \\ g\left(x_0\right) = g_0. \end{array}\right\} \tag{54}$$

The following expression is obtained by applying (54) of the numerical scheme:

$$k_1 = \frac{\hat{h}}{\Gamma\left(\vartheta+1\right)}g\left(x_t\right), \tag{55}$$

$$k_2 = \left(\frac{\hat{h}}{\Gamma\left(\vartheta+1\right)} + \left(\frac{\hat{h}}{\Gamma\left(\vartheta+1\right)}\right)^2\right)g\left(x_t\right), \tag{56}$$

$$k_3 = \left(\frac{\hat{h}}{\Gamma\left(\vartheta+1\right)} + \left(\frac{\hat{h}}{\Gamma\left(\vartheta+1\right)}\right)^2 + \frac{1}{2}\left(\frac{\hat{h}}{\Gamma\left(\vartheta+1\right)}\right)^3\right)g\left(x_t\right), \tag{57}$$

where $h^{\vartheta}\lambda = \hat{h}$. Now, using (55)-(57) in (40), we have the following stability polynomial:

$$Q\left(z\right) = \frac{g\left(x_{t+1}\right)}{g\left(x_t\right)} = \left(1 + \frac{z^2 + \left(z + z^2 + \frac{1}{2}z^3\right)^2}{2z + z^2 + \frac{1}{2}z^3}\right), \tag{58}$$

where $z = \frac{\hat{h}}{\Gamma(\vartheta+1)}$. Using MatLab software, the stability zone of $\mathrm{FEM}_1^{[*]} - \mathrm{FEM}_3^{[*]}$ and $\mathrm{FEM}_1^{[**]}$ are depicted for various values of ϑ given in Figs. 1-2, taking (58) into account. Figure 1(a) demonstrate that the newly proposed approach has a larger stability region compared to other existing fractional order approaches, $\mathrm{FEM}_1^{[*]}$-$\mathrm{FEM}_3^{[*]}$, while Fig. 1(b) illustrates the stability region of the proposed $\mathrm{FEM}_1^{[**]}$ technique for a range of fractional parameter values.

Table 1 shows the stability interval and region for various fractional parameter values, while Fig. 2(a-d) visualizes the stability surface generated by using:

$$\left|\frac{g\left(x_{t+1}\right)}{g\left(x_t\right)}\right| = Q\left(z\right) < 1. \tag{59}$$

The stability surface Fig. 2(a-d) and intervals (Table 1) clearly demonstrate that the newly developed fractional-order method is more stable and has a greater range of stability than the existing fractional order scheme. The recently suggested approach is a good substitute for existing fractional schemes with the same convergence order when solving fractional order schemes. The next section compares the efficiency, stability, and consistency of numerical approaches to existing methods by addressing a variety of engineering problems using fractional order differential equations as a result of mathematical formulation.

Numerical results

Numerical results of schemes for solving FOIVPs are critical in determining the efficiency and accuracy of the chosen approaches. Important results, including convergence rates, error estimates, and computing efficiency, shed light on the dependability and effectiveness of the schemes. These results help identify the most suitable methods for different types of problems and optimize their parameters. Moreover, numerical results allow a

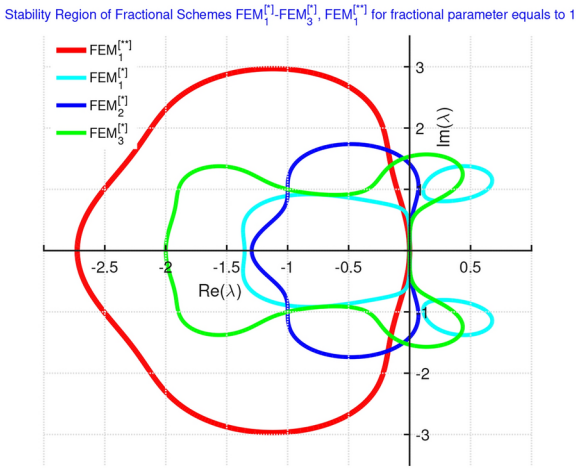

(a) Combine fractional schemes' stability region for $\vartheta = 1$

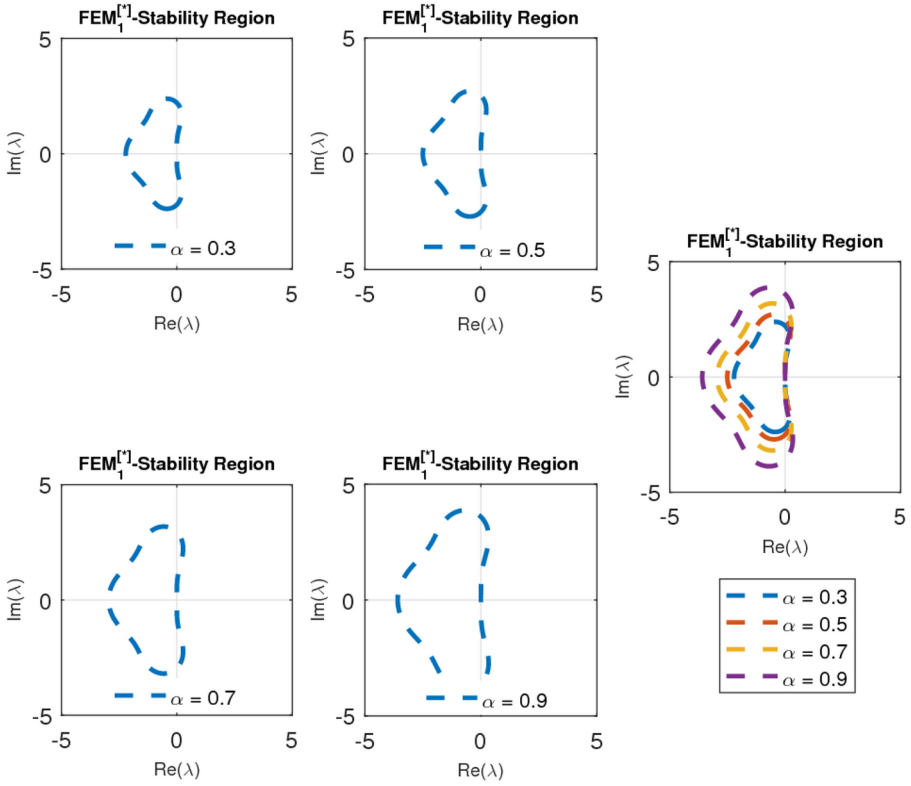

(b) The stability zone of $\text{FEM}_1^{[**]}$ for various fractional parameter values ϑ

Fig. 1. (**a**-**b**) Stability regions of the fractional schemes $\text{FEM}_1^{[*]}$-$\text{FEM}_3^{[*]}$ and $\text{FEM}_1^{[**]}$

direct comparison of different schemes for their strengths and weaknesses. We compare the efficiency of our newly created approaches to modern high-performance algorithms for fractional differential equations, such as Fractional Finite Difference[40], Domain Decomposition Method[41], and Fractional Chebyshev Spectral Method[42]. Ultimately, these findings contribute to the further refinement of schemes, ensuring their applicability in practical settings.

We illustrate how well the numerical schemes $\text{FEM}_1^{[*]} - \text{FEM}_3^{[*]}$ and $\text{FEM}_1^{[**]}$ perform numerically on a variety of FOIVPs, indicating their ability to tackle real-world problems.

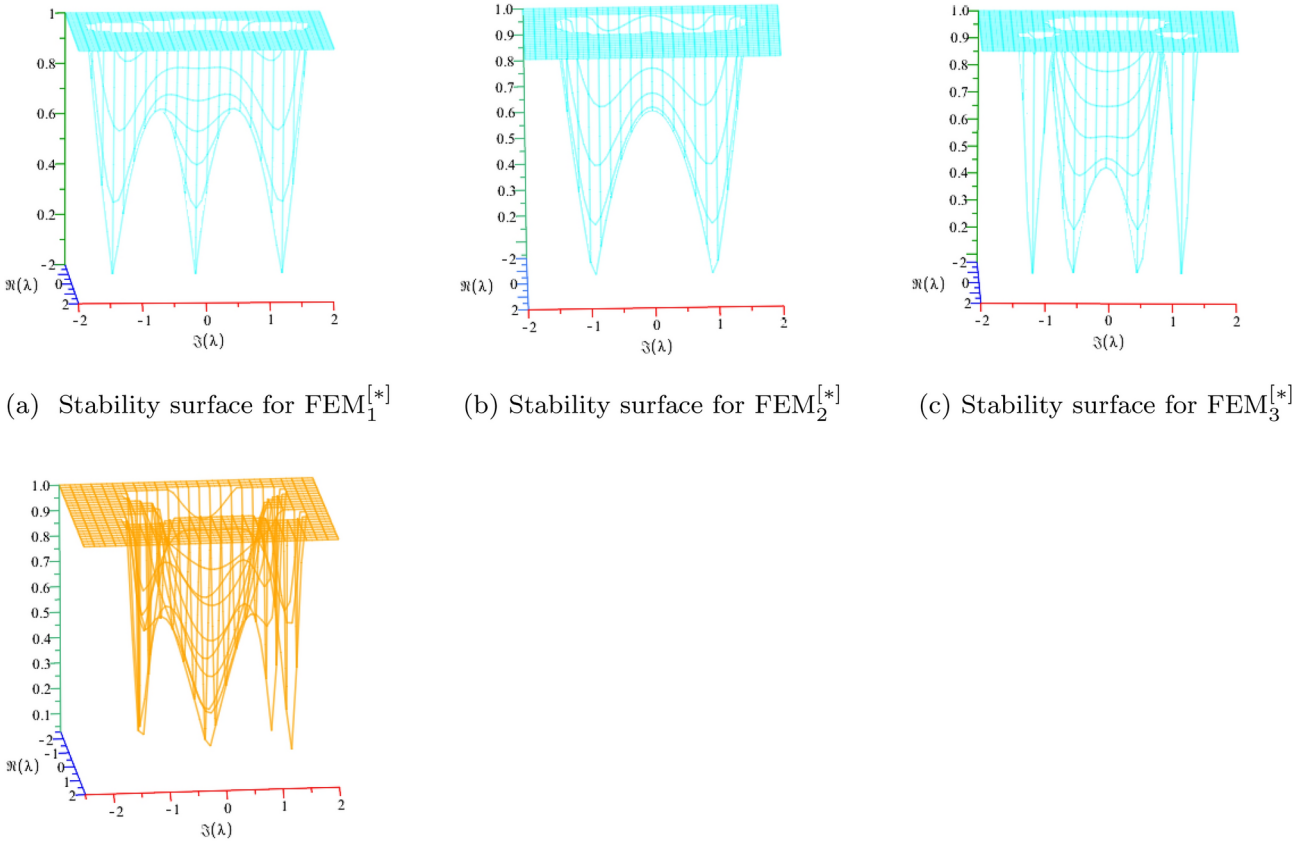

(a) Stability surface for $\mathrm{FEM}_1^{[*]}$ (b) Stability surface for $\mathrm{FEM}_2^{[*]}$ (c) Stability surface for $\mathrm{FEM}_3^{[*]}$

(d) Stability surface for $\mathrm{FEM}_1^{[**]}$

Fig. 2. (**a**-**d**) The stability surfaces of the fractional schemes $\mathrm{FEM}_1^{[*]}$-$\mathrm{FEM}_3^{[*]}$ and $\mathrm{FEM}_1^{[**]}$ using (59).

ϑ	$\mathrm{FEM}_1^{[*]}$	$\mathrm{FEM}_2^{[*]}$	$\mathrm{FEM}_3^{[*]}$	$\mathrm{FEM}_1^{[**]}$
0.1	$[-1.739479, 0]$	$[-1.490982, 0]$	$[-1.345604, -0.008016]$	$[-3.124353, -0.013026]$
0.3	$[-2.116232, 0]$	$[-1.490982, 0]$	$[-1.426854, -0.008016]$	$[-3.712425, -0.013026]$
0.5	$[-1.490982, 0]$	$[-1.695391, 0]$	$[-1.619238, -0.008016]$	$[-4.207415, -0.013026]$
0.7	$[-1.695391, 0]$	$[-1.995992, 0]$	$[-1.907816, -0.008016]$	$[-4.962926, -0.013026]$
0.9	$[-1.995992, 0]$	$[-2.422846, 0]$	$[-2.324649, -0.008016]$	$[-6.031062, -0.013026]$

Table 1. Comparison of the stability interval of fractional schemes $\mathrm{FEM}_1^{[**]}$,$\mathrm{FEM}_1^{[*]}-\mathrm{FEM}_3^{[*]}$ for solving fractional differential equations.

To analyze the accuracy of the suggested technique, we utilize the error formula:

$$\text{Max-Error} = \max_{t=0,1,\ldots,n} \|g(x_t) - g_t\|, \tag{60}$$

where $g(x_t)$ is the exact solution and g_t is the estimated solution at each grid point x_t. This metric provides a clear measure of the difference between the computed and exact solutions, allowing for a reliable evaluation of the method's precision. To attain optimal performance in fractional-order numerical schemes, we employ an adaptive step-size technique that dynamically modifies the step size based on local error estimates

$$Err = \|g(x_t) - g_t\|. \tag{61}$$

This method ensures precision while eliminating unnecessary computations. During each iteration, we calculate an estimated error, Err, and compare it to a predetermined absolute tolerance, Tol. The adaptive step-size strategy takes these steps:

- Step Acceptance: If $Err \leq Tol$, the computed step is accepted, and the step size is raised for faster computation while keeping accuracy.
- Step Rejection and Refinement: If $Err > Tol$, reject the computed step and change the step size to enhance accuracy before recalculating the the solution.

To update the step size, we use the following formula:

$$h_{new} = \eta^{[*]} \times h_{old} \left(\frac{Tol}{Err} \right)^{\frac{1}{\vartheta+1}}, \tag{62}$$

where *Tol* represents the predefined absolute tolerance, $\eta^{[*]} \in (0, 1)$ is an adjustment factor that avoids step-size failures. In order to minimize computational effort and attain the required accuracy level, this formula (62) enables us to modify the step-size according to the magnitude of the error. In (62), an additional ϑ is given to reflect the precision of the lower-order approach presented in (50).

The following notations are used for uniformity and clarity when referring to various numerical techniques and performance metrics throughout this section. These notations help to shorten discussions, making it easier to compare and assess different techniques' efficacy.

Notations

h: Step length
Exact: Exact solution of the FODES'
ϑ: Fractional parameter
$\eta^{[*]}$: Adjustment factor in adaptive step size strategy
Fun: Total number of functions evaluation
Max-Error: Maximum error
CPU-time: Computational time in seconds
$\|.\|_{\infty}$: Error norm
Avg_{∞}: Average error
MSE_{∞}: Mean square error norm
$\text{FFDM}^{[*]}$, $\text{FDDM}^{[*]}$: Fractional Finite Difference, Domain Decomposition Method
$\text{FCSM}^{[*]}$: Fractional Chebyshev Spectral Method
$\text{FEM}_1^{[*]} - \text{FEM}_3^{[*]}$: Existing fractional scheme
$\text{FEM}_1^{[**]}$: Newly developed fractional schemes for solving FOIVPs

Implementations of $\text{FEM}_1^{[*]} - \text{FEM}_3^{[*]}$, $\text{FEM}_1^{[**]}$:

The following Algorithms 1 and 2, demonstrate the constant and adaptive step size strategies for solving FOIVPs using both the proposed and existing fractional-order numerical schemes. These algorithms enable a systematic approach to applying and comparing various fractional order methods, ensuring a thorough assessment of their accuracy, efficiency, and stability in solving FOIVPs.

Steps	Description
1: Initialize	Define $D^{[\vartheta]}y(x) = f(x, y(x)); y^k\left(\theta_0^{[*]}\right) = y_0^k$, Read the initial values of (x_0 and g_0), the values of fractional parameter ϑ, number of steps (n) and end point. Choose the step size h=$(x_n - x_0)/n$
2: Start loop over time	Set $t = 0$
3: Compute k_1	$k_1 = f(x_t, g_t)$.
4: Compute k_2	$k_2 = f\left(x_t + \frac{h^{\vartheta}}{\Gamma(\vartheta+1)}, g_t + \frac{h^{\vartheta}}{\Gamma(\vartheta+1)} k_1\right)$.
5: Compute k_3	$k_3 = f\left(x_t + \frac{h^{\vartheta}}{\Gamma(\vartheta+1)}, g_t + \frac{h^{\vartheta}}{\Gamma(\vartheta+1)} \left(\frac{k_1+k_2}{2}\right)\right)$.
6: Update solution	$g_{t+1} = g_t + \frac{h^{\vartheta}}{\Gamma(\vartheta+1)} \frac{(k_1)^2 + (k_3)^2}{k_1+k_3}$. $g_t = g_0$. $t = t + 1$. while $t < n$ do Approximate solution g_t at discrete time points.
7: End loop	end while

Algorithm 1. Adoption of $\text{FEM}_1^{[**]}$ for solving FOIVPs with fixed step length.

Steps	Description
1: Initialize	Define $D^{[\vartheta]}y(x) = f(x, y(x)); y^k\left(\theta_0^{[*]}\right) = y_0^k$, Choose initial step size h_0, the values of fractional parameter ϑ, error tolerance Tol, and set $x_t = x_0$
2: Start loop over time	while $t < N$ do
3: Compute k_1	$k_1 = f(x_t, g_t)$.
4: Compute k_2	$k_2 = f\left(x_t + \frac{h^\vartheta}{\Gamma(\vartheta+1)}, g_t + \frac{h^\vartheta}{\Gamma(\vartheta+1)}k_1\right)$.
5: Compute k_3	$k_3 = f\left(x_t + \frac{h^\vartheta}{\Gamma(\vartheta+1)}, g_t + \frac{h^\vartheta}{\Gamma(\vartheta+1)}\left(\frac{k_1+k_2}{2}\right)\right)$.
6: Compute tentative solution	$g_{t+1} = g_t + \frac{h^\vartheta}{\Gamma(\vartheta+1)}\frac{(k_1)^2+(k_3)^2}{k_1+k_3}$.
7: Estimate local error	Compute error error norm $Err = \|.\|_\infty$
8: Adjust step size	$t = t + 1$.
9: Accept or reject step	If $Err > Tol$, reduce h; if Err<Tol/2; increase h; Use:$h_{new} = \eta^{[*]} \times h_{old}\left(\frac{Tol}{Err}\right)^{\frac{1}{\vartheta+1}}$. If $Err \le Tol$, accept $g_{t+1} = g_t$and update $x_t = x_0 + h$, otherwise, recompute with new h.
10: End loop	end while
11: Output	Approximate solution g_t at adaptive time steps.

Algorithm 2. Adoption of $\mathrm{FEM}_1^{[**]}$ for solving FOIVPs with adaptive step size strategy.

Example 1:[43]

Fractional differential equations have many applications in engineering because they can simulate complicated systems with memory and hereditary features. They are used in control engineering to create reliable controllers for dynamic systems. FODEs characterize the time-varying relationships between stress and strain in viscoelastic materials. They are crucial for simulating anomalous diffusion processes in mass and heat transfer. Electrical engineers use FODEs to improve circuit design and signal processing.In industrial engineering, they are particularly valuable for fault identification and predictive maintenance because they capture the non-linear and time-dependent behavior that occurs in turbulent flows, frequently giving rise to the following FOIVPs-I:

$$\left.\begin{array}{c} D^{[\vartheta]}y(x) = \frac{\Gamma(2\vartheta+1)}{\Gamma(\vartheta+1)}x^\vartheta - \frac{2}{\Gamma(3-\vartheta)}x^{2-\vartheta} + \left(x^{2\vartheta} - x^2\right) - (y(x))^4, \\ y(0) = 0, \quad x > 0 \end{array}\right\} \tag{63}$$

and $\vartheta \in (0, 1]$. The exact solution of (63) is $y(x) = x^{2\vartheta} - x^2$.

Table 2, illustrates the numerical results of the fractional schemes with a fixed step length of h= 0.1. The exact solution of the FOIVPs-I for various values of x and $\vartheta = 0.9$ is displayed in the second column of Table 2.

Tables 3 and 4 show the fractional scheme's numerical results for a range of x values for $\vartheta = 0.9$. The numerical schemes' consistency analysis is displayed in Tables 5 and 6. In Tables 5 and 6, CPU-time shows the processing time in seconds, Fun, indicates the total number of function evaluations and Max-Error, indicates the maximum errors. In terms of consistency, the newly developed method $\mathrm{FEM}_1^{[**]}$ is more stable, as its local error

x	Exact	$\mathrm{FEM}_1^{[*]}$	$\mathrm{FEM}_2^{[*]}$	$\mathrm{FEM}_3^{[*]}$	$\mathrm{FEM}_1^{[**]}$
0.0	0.0	0.0	0.0	0.0	0.0
0.4	0.00295929	0.00824357	0.0030682	0.0030682	0.00278798
0.8	0.00286267	0.00299866	0.0030196	0.0030496	0.00312646
1.2	−0.0052413	−0.0054431	−0.005197	−0.005197	−0.0044777
1.6	−0.0239515	−0.0256857	−0.024298	−0.024298	−0.0228216
2.0	−0.0550696	−0.0566784	−0.056184	−0.056184	−0.0538415

Table 2. Comparison of exact and approximate solutions of fractional schemes FOIVPs-I using a step length of h=0.1.

x	$\mathrm{FEM}_1^{[*]}$	$\mathrm{FEM}_2^{[*]}$	$\mathrm{FEM}_3^{[*]}$	$\mathbf{FEM}_1^{[**]}$
0.0	0.0	0.0	2.5549×10^{-4}	0.0
0.4	2.84170×10^{-4}	4.61359×10^{-5}	1.09084×10^{-4}	2.5549×10^{-4}
0.8	1.35991×10^{-4}	8.79336×10^{-3}	1.56958×10^{-4}	2.6336×10^{-4}
1.2	1.23852×10^{-3}	1.56956×10^{-4}	1.28997×10^{-3}	5.1994×10^{-5}
1.6	7.33445×10^{-3}	3.46699×10^{-3}	3.46993×10^{-3}	1.1314×10^{-5}
2.0	1.60938×10^{-3}	1.11148×10^{-3}	1.11148×10^{-3}	1.2285×10^{-5}

Table 3. Error comparison of fractional schemes $\mathrm{FEM}_1^{[**]}$,$\mathrm{FEM}_1^{[*]}-\mathrm{FEM}_3^{[*]}$ for solving FOIVPs-I using a step length of h=0.1.

x	$\mathrm{FEM}_1^{[*]}$	$\mathrm{FEM}_2^{[*]}$	$\mathrm{FEM}_3^{[*]}$	$\mathbf{FEM}_1^{[**]}$
0.0	0.0	0.0	2.5549×10^{-4}	0.0
0.4	2.84170×10^{-4}	4.61359×10^{-5}	1.09084×10^{-4}	2.5549×10^{-4}
0.8	1.35991×10^{-4}	8.79336×10^{-3}	1.56958×10^{-4}	2.6336×10^{-4}
1.2	1.23852×10^{-5}	1.56956×10^{-4}	1.28997×10^{-3}	5.1994×10^{-4}
1.6	7.33445×10^{-5}	3.46699×10^{-3}	3.46993×10^{-3}	1.1314×10^{-3}
2.0	1.60938×10^{-5}	1.11148×10^{-3}	1.11148×10^{-3}	1.2285×10^{-3}

Table 4. Error comparison of fractional schemes $\mathrm{FEM}_1^{[**]}$,$\mathrm{FEM}_1^{[*]}-\mathrm{FEM}_3^{[*]}$ for solving FOIVPs-I using a step length of h=0.025.

Parameter		**Step length 0.1**		
Schemes	$\mathrm{FEM}_1^{[*]}$	$\mathrm{FEM}_2^{[*]}$	$\mathrm{FEM}_3^{[*]}$	$\mathrm{FEM}_1^{[**]}$
Fun	25	27	40	40
Max-Error	7.3×10^{-3}	3.4×10^{-3}	3.4×10^{-3}	2.5×10^{-4}
CPU-Time	0.1×10^{-4}	1.1×10^{-3}	2.1×10^{-3}	0.2×10^{-4}

Table 5. Consistency analysis of fractional schemes for FOIVPs-I.

Parameter		**Step length 0.025**		
Schemes	$\mathrm{FEM}_1^{[*]}$	$\mathrm{FEM}_2^{[*]}$	$\mathrm{FEM}_3^{[*]}$	$\mathrm{FEM}_1^{[**]}$
Fun	25	27	40	40
Max-Error	1.6×10^{-4}	4.6×10^{-5}	1.0×10^{-4}	2.5×10^{-4}
CPU-Time	0.1×10^{-4}	1.1×10^{-3}	2.1×10^{-3}	3.2×10^{-3}

Table 6. Consistency analysis of fractional schemes for FOIVPs-I.

is lower than that of $\mathrm{FEM}_1^{[*]}$-$\mathrm{FEM}_3^{[*]}$. It is also more consistent because its CPU time, total number of function evaluations, and local error are all lower than those of earlier methods. In Fig. 3, the exact and approximate solutions are shown along with the corresponding error.

We employ the adaptive step size strategy to examine the behavior and improve the rate of convergence of the numerical schemes of fractional order. By selecting alternative tolerances, i.e., $\in = 10^{-2}, 10^{-4}$ and 10^{-6}, we can enhance the consistency of the numerical schemes. The results of the numerical schemes are shown in Tables 7, 8, 9.

In Tables 7-9, we calculated the error using various stopping criteria and the computational time in seconds using the common tic-toc function in Matlab. These tables show that our newly developed method outperforms others in terms of the $\|.\|_\infty$-error norm, Avg_∞-error norm, $\mathrm{MSE}_\infty-$ mean square error norm, and CPU time. This indicates better convergence behavior and suggests a superior alternative for solving fractional differential equations. Fig. 3 also displays the exact and approximate solution for fixed step-length h, as well as the error graph, for various fractional parameter values ϑ. Figure 3(a, b) compare the exact and approximate solutions using $\mathrm{FEM}_1^{[**]}$ and $\mathrm{FEM}_1^{[*]}-\mathrm{FEM}_3^{[*]}$ for various tolerance levels utilizing an adaptive step size technique. As the tolerance increases from 10^{-2} to 10^{-6}, Fig. 4(a-f) clearly shows that the accuracy of the method improves.

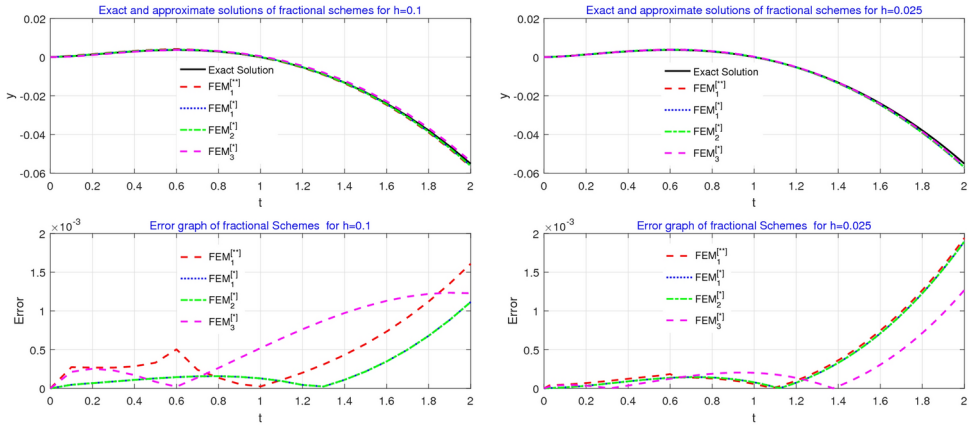

(a) Exact and approximate solutions with error graph for h=0.1.

(b) Exact and approximate solutions with error graph for h=0.025.

Fig. 3. (**a**-**b**) Comparison of the exact and approximate solutions of the fractional numerical methods for h=0.1 and h=0.025 to solve FOIVPs-I.

Parameter		$\in = 10^{-2}$		
Schemes	$\|\cdot\|_\infty$	Avg_∞	MSE_∞	**CPU-time**
$\text{FEM}_1^{[*]}$	1.36×10^{-2}	5.05×10^{-3}	9.96×10^{-3}	0.0123124
$\text{FEM}_2^{[*]}$	9.65×10^{-2}	7.66×10^{-2}	8.56×10^{-3}	0.0234233
$\text{FEM}_3^{[*]}$	1.05×10^{-2}	9.56×10^{-2}	1.64×10^{-2}	0.0342424
$\text{FEM}_1^{[**]}$	0.61×10^{-3}	1.05×10^{-3}	0.12×10^{-4}	0.0065232

Table 7. Adaptive step size for solving FOIVPs-I using fractional schemes $\text{FEM}_1^{[*]} - \text{FEM}_3^{[*]}, \text{FEM}_1^{[**]}$.

Parameter		$\in = 10^{-4}$		
Schemes	$\|\cdot\|_\infty$	Avg_∞	MSE_∞	**CPU-time**
$\text{FEM}_1^{[*]}$	5.98×10^{-3}	4.60×10^{-3}	4.23×10^{-3}	2.5×10^{-4}
$\text{FEM}_2^{[*]}$	6.09×10^{-4}	0.60×10^{-3}	0.56×10^{-3}	2.5×10^{-4}
$\text{FEM}_3^{[*]}$	8.87×10^{-3}	9.34×10^{-3}	7.45×10^{-4}	2.5×10^{-4}
$\text{FEM}_1^{[**]}$	0.16×10^{-4}	1.87×10^{-4}	2.17×10^{-5}	3.2×10^{-3}

Table 8. Adaptive step size for solving FOIVPs-I using fractional schemes $\text{FEM}_1^{[*]} - \text{FEM}_3^{[*]}, \text{FEM}_1^{[**]}$.

Parameter		$\in = 10^{-6}$		
Schemes	$\|\cdot\|_\infty$	Avg_∞	MSE_∞	**CPU-time**
$\text{FEM}_1^{[*]}$	1.24×10^{-3}	9.98×10^{-6}	2.19×10^{-6}	5.5×10^{-4}
$\text{FEM}_2^{[*]}$	6.03×10^{-4}	4.66×10^{-5}	1.87×10^{-4}	7.7×10^{-5}
$\text{FEM}_3^{[*]}$	0.17×10^{-4}	1.51×10^{-4}	6.71×10^{-3}	6.7×10^{-5}
$\text{FEM}_1^{[**]}$	0.37×10^{-6}	1.72×10^{-6}	2.15×10^{-6}	1.2×10^{-6}

Table 9. Adaptive step size for solving FOIVPs-I using fractional schemes $\text{FEM}_1^{[*]} - \text{FEM}_3^{[*]}, \text{FEM}_1^{[**]}$.

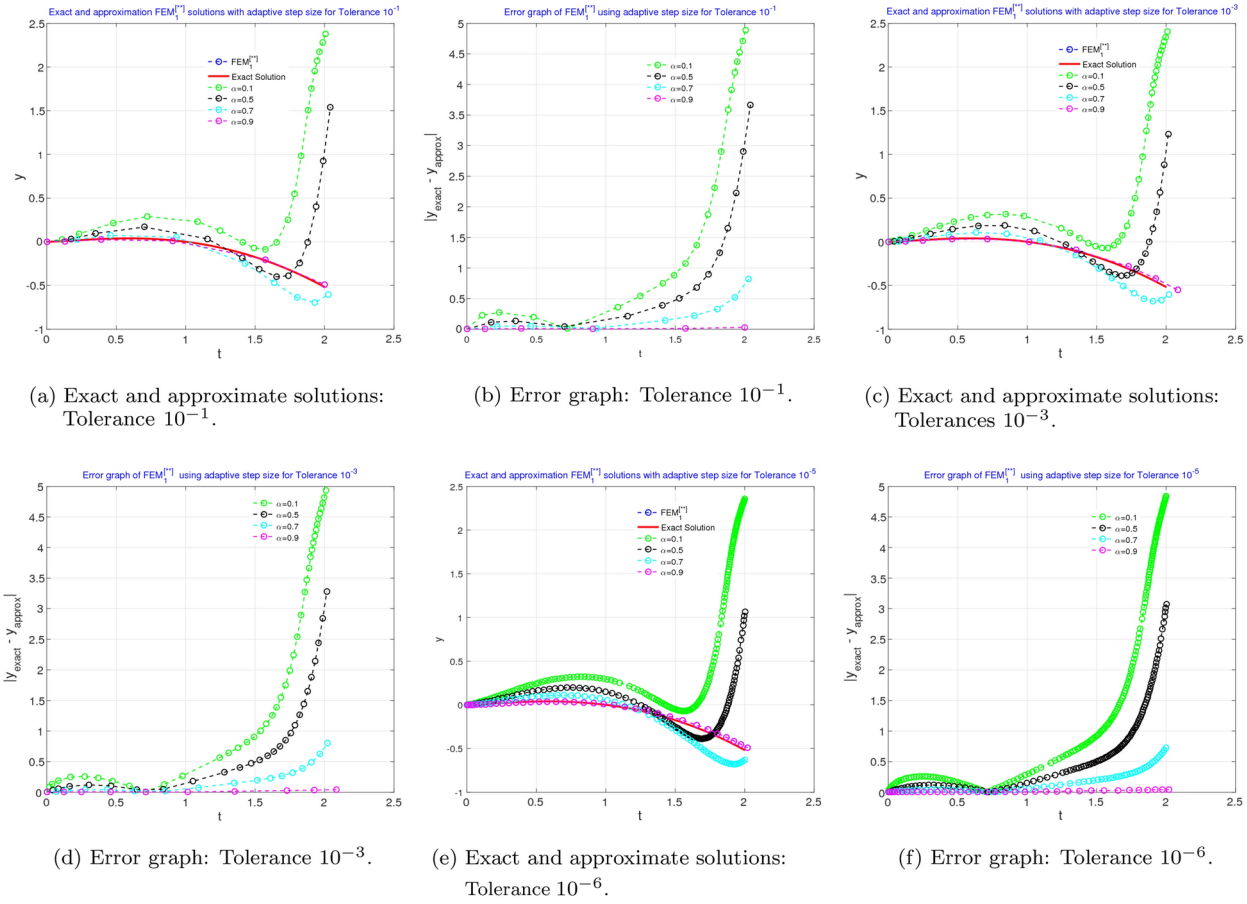

(a) Exact and approximate solutions: Tolerance 10^{-1}.

(b) Error graph: Tolerance 10^{-1}.

(c) Exact and approximate solutions: Tolerances 10^{-3}.

(d) Error graph: Tolerance 10^{-3}.

(e) Exact and approximate solutions: Tolerance 10^{-6}.

(f) Error graph: Tolerance 10^{-6}.

Fig. 4. (**a**-**f**) Comparison of the exact and approximate solutions, along with error graphs, utilizing adaptive step size strategy for solving FOIVPs-I using $\mathrm{FEM}_1^{[**]}$ and $\mathrm{FEM}_1^{[*]}$-$\mathrm{FEM}_3^{[*]}$ respectively.

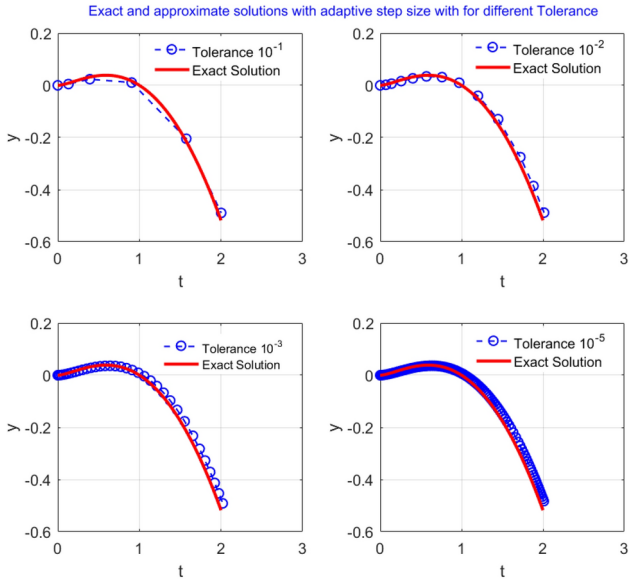

Fig. 5. Comparison of exact and approximate solutions using adaptive step length leveraging $\mathrm{FEM}_1^{[**]}$ to solve FOIVPs-I with varying tolerances.

Tolerance		$\in = 10^{-6}$		
Schemes	$\mathrm{FEM}_1^{[**]}$	$\mathrm{FFDM}^{[*]}$	$\mathrm{FDDM}^{[*]}$	$\mathrm{FCSM}^{[*]}$
MSE_∞	1.24×10^{-6}	9.98×10^{-3}	2.19×10^{-2}	5.5×10^{-4}
CPU-time	0.3772×10^{-3}	5.7244×10^{-3}	6.4552×10^{-2}	1.2439×10^{-2}

Table 10. Efficiency comparison with contemporary high-performance algorithms.

x	Exact	$\mathrm{FEM}_1^{[*]}$	$\mathrm{FEM}_2^{[*]}$	$\mathrm{FEM}_3^{[*]}$	$\mathrm{FEM}_1^{[**]}$
0.0	0.0	0.0	0.0	0.0	0.0
0.4	0.16147	0.18018	0.16375	0.16329	0.161375
0.8	0.64143	0.66193	0.64935	0.64724	0.6414283
1.2	1.43741	1.45274	1.44736	1.44664	1.4374135
1.6	2.64813	2.55723	2.55525	2.56786	2.6483475
2.0	3.97254	3.97594	3.97586	4.41035	3.9725656

Table 11. Comparison of exact and approximate solutions of fractional schemes FOIVPs-II using a step length of h=0.1.

However, as the tolerance increases, the number of functions computed and CPU time increase significantly. The convergence rate, or higher accuracy obtained, improves in comparison to fixed-step length. Using an adaptive step size strategy, Tables 7-9 demonstrate unequivocally that the newly designed fractional scheme outperforms the existing approaches $\mathrm{FEM}_1^{[*]}$-$\mathrm{FEM}_3^{[*]}$ in terms of stability and consistency. Figure 5 depicts the exact and approximate solutions for various tolerances using an adaptive step size strategy, indicating that as the tolerance increases, the approximate solutions correspond more closely to the precise solution for $\vartheta = 0.9$.

We evaluate the efficiency of our newly developed method in comparison to existing high-performance algorithms for fractional differential equations, as demonstrated in Table 10.

Table 10, presents the numerical results of $\mathrm{FEM}_1^{[*]}$, $\mathrm{FFDM}^{[*]}$, $\mathrm{FDDM}^{[*]}$, and $\mathrm{FCSM}^{[*]}$ for solving FOIVPs-I. In terms of CPU-time and MSE, our newly developed approaches $\mathrm{FEM}_1^{[**]}$, outperform $\mathrm{FFDM}^{[*]}$, $\mathrm{FDDM}^{[*]}$, and $\mathrm{FCSM}^{[*]}$.

Example 2:[44]

In biomedical engineering, FODEs are increasingly being used because they may able to be more accurately replicate complex, real-world scenarios than standard integer-order models. They are employed to investigate abnormal diffusion pathways in biological tissues to better understand tissue engineering and drug delivery. The viscoelastic properties of biological materials, such as cartilage and soft tissues, are also represented by FDEs. They enhance cardiac electrophysiology modeling of irregular rhythms and heart tissue conductivity. They also contribute to our understanding of neural network signal processing and tumor growth dynamics. In these applications, FODEs' capacity to capture memory and hereditary effects found in biological systems is modeled by the following FOIVPs-II:

$$\left.\begin{array}{c} D^{[\vartheta]}y(x) + 2\left(y(x)\right)^2 = \Gamma\left(\vartheta+2\right)x + 2\left(x^{\vartheta+1}\right)^2, \\ y\left(0\right) = 0, \quad x > 0 \end{array}\right\} \tag{64}$$

and $\vartheta \in (0, 1]$. The exact solution of (64) is $y(x) = x^{\vartheta+1}$.

Table 11, illustrates the numerical results of the fractional schemes with a fixed step length of $h = 0.1$. The exact solution of the FOIVPs-II for various values of x and $\vartheta = 0.9$ is displayed in the second column of Table 11. Figure 6 illustrates the exact and approximate solutions for $\vartheta = 0.9$.

The numerical results of the fractional scheme are displayed in Tables 12 and 13 for various values of x for $\vartheta = 0.9$. The consistency analysis of the numerical schemes is shown in Tables 14 and 15. In Tables 14 and 15, Fun denotes the total number of function evaluations, Max-Error represents the maximum errors, and CPU-time displays the processing time in seconds. In terms of consistency, the recently created methods are more stable because the local error is lower than that of $\mathrm{FEM}_1^{[*]}-\mathrm{FEM}_3^{[*]}$, and they are more consistent since the local error, total number of function evaluations, and CPU time are lower than those of previous methods.

Using the adaptive step size strategy, we can improve the convergence rate and examine the behavior of the fractional order numerical schemes. By selecting alternative tolerances, i.e., $\in = 10^{-2}, 10^{-4}$ and 10^{-5} , we can enhance the consistency of the numerical schemes. The results of the numerical schemes are shown in Tables 16, 17, 18.

Tables 16-18, show the computational duration in seconds using the common tic-toc function in Matlab and the error using various stopping criteria. These tables demonstrate that our newly developed method outperforms others in terms of $\|.\|_\infty$-error norm, Avg_∞ -error norm, $\mathrm{MSE}_\infty-$mean square error norm, and CPU time. This suggests better convergence behavior and a superior alternative for solving fractional differential equations. Figure 6(a) displays the exact and approximate solutions, as well as the error graph in Fig. 6(b), for

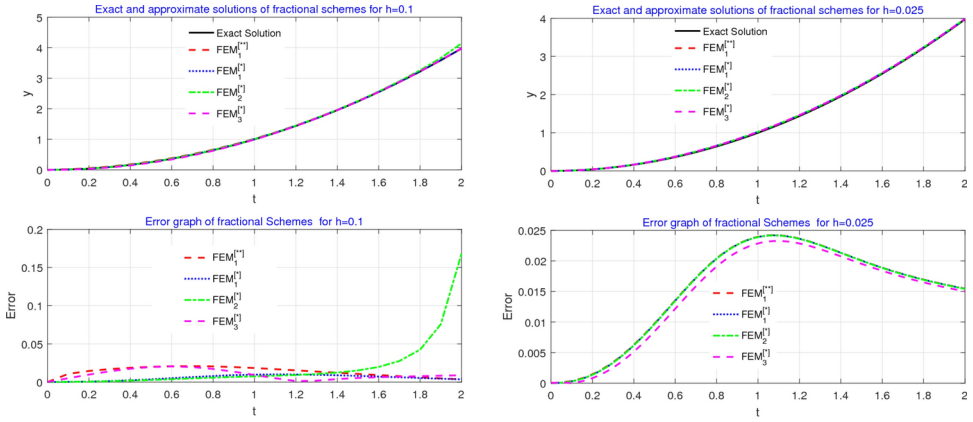

(a) Exact and approximate solutions with error graph for h=0.1.

(b) Exact and approximate solutions with error graph for h=0.025.

Fig. 6. (**a**-**b**) Comparison of the exact and approximate solutions of the fractional numerical methods for h=0.1 and h=0.025 to solve FOIVPs-II.

x	$\mathrm{FEM}_1^{[*]}$	$\mathrm{FEM}_2^{[*]}$	$\mathrm{FEM}_3^{[*]}$	$\mathbf{FEM}_1^{[**]}$
0.0	0.0	0.0	2.5549×10^{-4}	0.0
0.4	2.84170×10^{-3}	4.61359×10^{-5}	1.09084×10^{-4}	2.0549×10^{-4}
0.8	1.35991×10^{-4}	8.79336×10^{-3}	1.56958×10^{-4}	2.1336×10^{-4}
1.2	1.23852×10^{-5}	1.56956×10^{-4}	1.28997×10^{-3}	5.1994×10^{-4}
1.6	7.33445×10^{-5}	3.46699×10^{-3}	3.46993×10^{-3}	1.1314×10^{-5}
2.0	1.60938×10^{-5}	1.11148×10^{-3}	1.11148×10^{-3}	1.2285×10^{-5}

Table 12. Error comparison of fractional schemes $\mathrm{FEM}_1^{[*]} - \mathrm{FEM}_3^{[*]}$, and $\mathrm{FEM}_1^{[**]}$ for solving FOIVPs-II using a step length of h=0.1.

x	$\mathrm{FEM}_1^{[*]}$	$\mathrm{FEM}_2^{[*]}$	$\mathrm{FEM}_3^{[*]}$	$\mathbf{FEM}_1^{[**]}$
0.0	1.00323×10^{-2}	1.87565×10^{-2}	2.53458×10^{-4}	1.65454×10^{-2}
0.4	9.56467×10^{-2}	9.87567×10^{-1}	1.64365×10^{-1}	0.3563878×10^{-2}
0.8	4.35454×10^{-1}	9.35678×10^{-2}	0.75765×10^{-1}	2.6467877×10^{-2}
1.2	7.64544×10^{-1}	1.76454×10^{-2}	3.45643×10^{-2}	9.4674567×10^{-4}
1.6	9.64546×10^{-1}	3.85665×10^{-1}	9.64356×10^{-2}	0.3564637×10^{-2}
2.0	8.64543×10^{-1}	1.87456×10^{-2}	6.36735×10^{-1}	1.6435646×10^{-3}

Table 13. Error comparison of fractional schemes $\mathrm{FEM}_1^{[**]}$,$\mathrm{FEM}_1^{[*]} - \mathrm{FEM}_3^{[*]}$ for solving FOIVP-II using a step length of h=0.025.

Parameters		**Step length 0.1**		
Schemes	$\mathrm{FEM}_1^{[*]}$	$\mathrm{FEM}_2^{[*]}$	$\mathrm{FEM}_3^{[*]}$	$\mathrm{FEM}_1^{[**]}$
Fun	21	22	40	40
Max-Error	2.8×10^{-3}	8.7×10^{-3}	3.4×10^{-3}	2.1×10^{-4}
CPU-time	0.5×10^{-3}	4.7×10^{-3}	2.2×10^{-3}	3.2×10^{-3}

Table 14. Consistency analysis of fractional schemes for FOIVPs-II.

Parameter		Step length 0.025		
Schemes	$\mathrm{FEM}_1^{[*]}$	$\mathrm{FEM}_2^{[*]}$	$\mathrm{FEM}_3^{[*]}$	$\mathrm{FEM}_1^{[**]}$
Fun	170	155	160	89
Max-Error	7.0×10^{-1}	2.1×10^{-1}	2.2×10^{-1}	2.5×10^{-2}
CPU-Time	5.7×10^{-4}	1.9×10^{-3}	9.7×10^{-3}	6.5×10^{-3}

Table 15. Consistency analysis of fractional schemes for FOIVPs-II.

Parameter		$\in = 10^{-2}$		
Schemes	$\|\cdot\|_\infty$	Avg_∞	MSE_∞	CPU-time
$\mathrm{FEM}_1^{[*]}$	0.54×10^{-1}	4.12×10^{-3}	6.23×10^{-3}	1.25×10^{-3}
$\mathrm{FEM}_2^{[*]}$	7.04×10^{-3}	0.32×10^{-2}	6.22×10^{-2}	9.15×10^{-3}
$\mathrm{FEM}_3^{[*]}$	0.21×10^{-2}	0.42×10^{-3}	2.34×10^{-3}	0.54×10^{-3}
$\mathrm{FEM}_1^{[**]}$	1.15×10^{-3}	1.07×10^{-4}	1.07×10^{-3}	0.12×10^{-3}

Table 16. Adaptive step size for solving FOIVPs-II using fractional schemes $\mathrm{FEM}_1^{[*]} - \mathrm{FEM}_3^{[*]}, \mathrm{FEM}_1^{[**]}$.

Parameter		$\in = 10^{-4}$		
Schemes	$\|\cdot\|_\infty$	Avg_∞	MSE_∞	CPU-time
$\mathrm{FEM}_1^{[*]}$	8.84×10^{-3}	0.12×10^{-3}	6.81×10^{-3}	1.11×10^{-3}
$\mathrm{FEM}_2^{[*]}$	3.99×10^{-3}	5.02×10^{-4}	7.11×10^{-4}	9.13×10^{-4}
$\mathrm{FEM}_3^{[*]}$	3.81×10^{-3}	9.34×10^{-3}	3.04×10^{-3}	0.59×10^{-3}
$\mathrm{FEM}_1^{[**]}$	3.95×10^{-4}	8.56×10^{-4}	9.80×10^{-5}	3.22×10^{-4}

Table 17. Adaptive step size for solving FOIVPs-II using fractional schemes $\mathrm{FEM}_1^{[*]} - \mathrm{FEM}_3^{[*]}, \mathrm{FEM}_1^{[**]}$.

Parameter		$\in = 10^{-6}$		
Schemes	$\|\cdot\|_\infty$	Avg_∞	MSE_∞	CPU-time
$\mathrm{FEM}_1^{[*]}$	0.76×10^{-4}	6.23×10^{-4}	8.43×10^{-4}	1.67×10^{-3}
$\mathrm{FEM}_2^{[*]}$	8.34×10^{-6}	0.33×10^{-5}	6.76×10^{-5}	9.15×10^{-4}
$\mathrm{FEM}_3^{[*]}$	1.76×10^{-4}	9.23×10^{-5}	0.23×10^{-4}	0.84×10^{-4}
$\mathrm{FEM}_1^{[**]}$	0.32×10^{-6}	5.65×10^{-6}	1.53×10^{-6}	1.37×10^{-5}

Table 18. Adaptive step size for solving FOIVPs-II using fractional schemes $\mathrm{FEM}_1^{[*]} - \mathrm{FEM}_3^{[*]}, \mathrm{FEM}_1^{[**]}$.

various fractional parameter values. Figure 6(a, b) compare the exact solution and approximate solutions using $\mathrm{FEM}_1^{[**]}$ and $\mathrm{FEM}_1^{[*]} - \mathrm{FEM}_3^{[*]}$ for various tolerance levels utilizing an adaptive step size technique. Figure 7(a-f) shows that increasing the tolerance from 10^{-2} to 10^{-6} improves the accuracy of the method. However, this also increases the number of function evaluations and CPU time, resulting in a higher convergence rate and higher accuracy compared to fixed-step lengths. Tables 16-18 clearly illustrate that the newly devised fractional scheme outperforms existing approaches $\mathrm{FEM}_1^{[*]} - \mathrm{FEM}_3^{[*]}$ in terms of stability and consistency when employing an adaptive step size strategy. Figure 8 depicts the exact and approximate solutions for various tolerances using an adaptive step size strategy, indicating that as the tolerance increases, the approximate solutions correspond more closely to the exact solution for $\vartheta = 0.9$.

The significance of our newly developed method is demonstrated through a comparison with contemporary high-performance methods for fractional differential equations, as illustrated in Table 19.

Table 19, presents the numerical results of $\mathrm{FEM}_1^{[*]}$, $\mathrm{FFDM}^{[*]}$, $\mathrm{FDDM}^{[*]}$, and $\mathrm{FCSM}^{[*]}$ for solving FOIVPs-II. In terms of CPU-time and MSE, our newly developed approaches $\mathrm{FEM}_1^{[**]}$ outperform, $\mathrm{FFDM}^{[*]}$, $\mathrm{FDDM}^{[*]}$, and $\mathrm{FCSM}^{[*]}$.

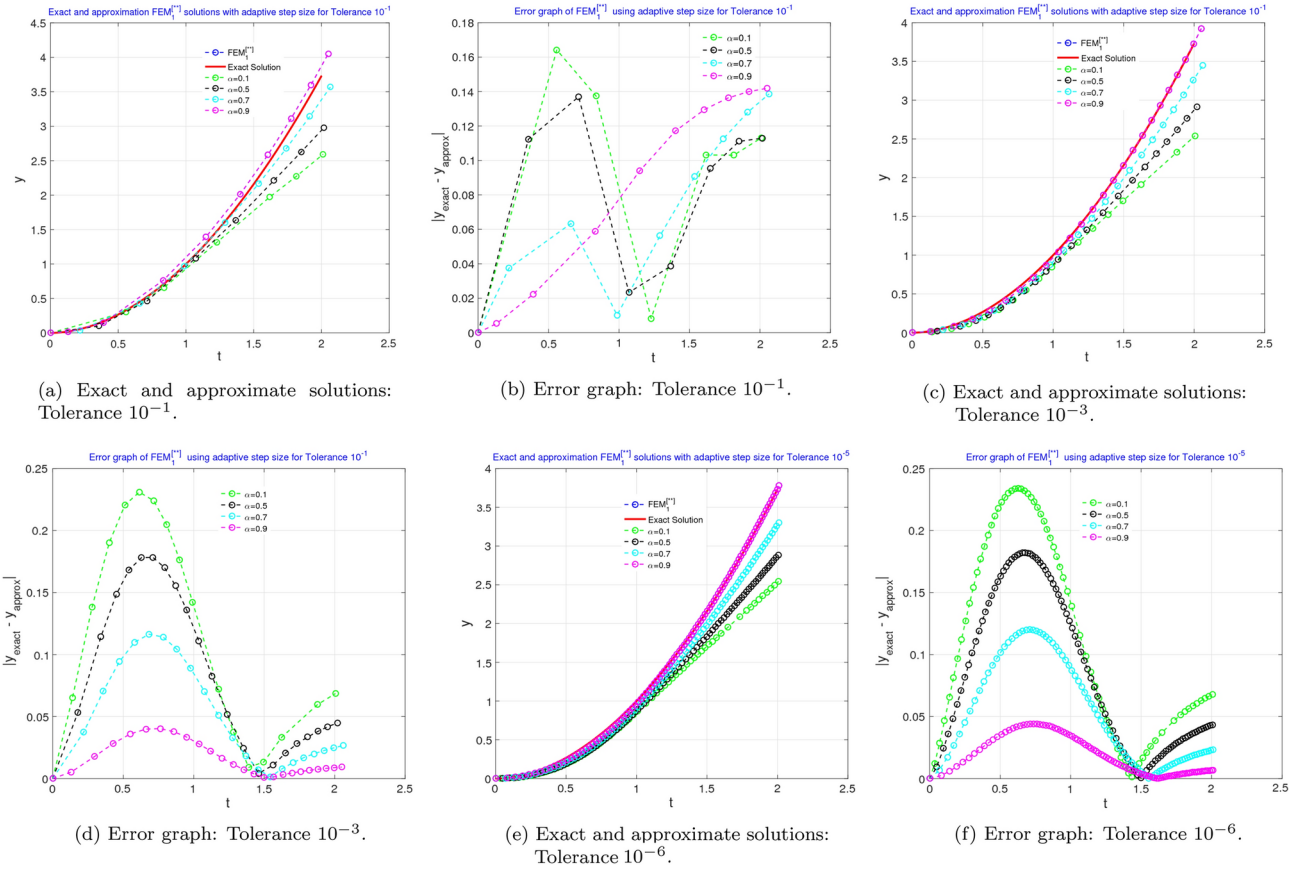

(a) Exact and approximate solutions: Tolerance 10^{-1}.

(b) Error graph: Tolerance 10^{-1}.

(c) Exact and approximate solutions: Tolerance 10^{-3}.

(d) Error graph: Tolerance 10^{-3}.

(e) Exact and approximate solutions: Tolerance 10^{-6}.

(f) Error graph: Tolerance 10^{-6}.

Fig. 7. (**a**-**f**) Comparison of the exact and approximate solutions, along with error graphs, utilizing adaptive step size strategy for solving FOIVPs-II using $\mathrm{FEM}_1^{[**]}$ and $\mathrm{FEM}_1^{[*]}$-$\mathrm{FEM}_3^{[*]}$ respectively.

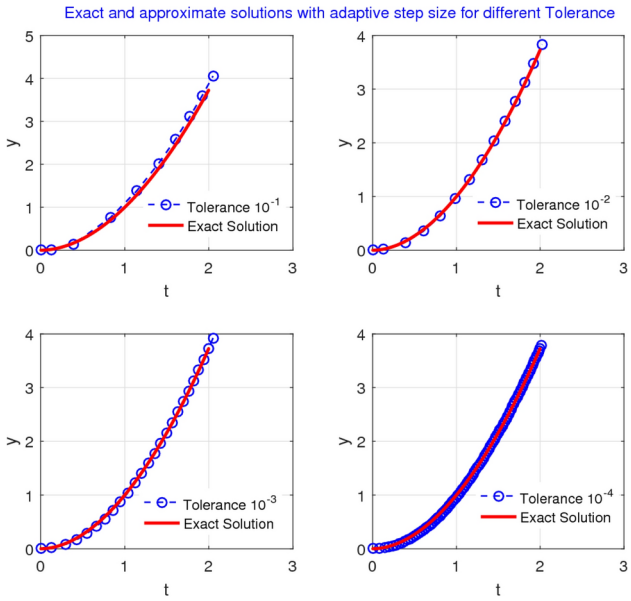

Fig. 8. Comparison of exact and approximate solutions using adaptive step length leveraging $\mathrm{FEM}_1^{[**]}$ to solve FOIVPs-II with varying tolerances.

Tolerance		$\in = 10^{-6}$		
Schemes	$\text{FEM}_1^{[**]}$	$\text{FFDM}^{[*]}$	$\text{FDDM}^{[*]}$	$\text{FCSM}^{[*]}$
MSE_∞	2.69×10^{-6}	0.13×10^{-2}	5.09×10^{-3}	0.51×10^{-2}
CPU-time	0.9012×10^{-4}	0.5986×10^{-3}	8.002×10^{-3}	9.653×10^{-3}

Table 19. Comparing efficiency against modern high-performance algorithms.

Physical significance of the numerical results

The numerical results highlight the physical importance of the developed fractional-order schemes, as they effectively capture the memory and heredity behaviors inherent in most practical systems described by fractional differential equations. The new fractional-order schemes' improved stability, accuracy, and precision make them perfect for simulating biological processes, anomalous diffusion, and viscoelasticity—areas where fractional-order models more accurately capture reality than standard integer-order models. The physical significance of the obtained results can be emphasized as follows:

- *Accurate Interpretation of Memory Effects:* The proposed fractional schemes accurately represent the memory and hereditary properties of fractional-order systems, which are important for representing real-world phenomena such as anomalous diffusion, viscoelastic materials, and biological processes.
- *Enhanced Precision with Fixed Step Size:* The approach produces more exact answers than current fractional schemes with fixed step size, as shown in Tables 2-5 and 11-15, which can be used to tackle fractional-order problems. This illustrates the scheme's capacity to model long-term physical processes such as heat conduction in fractals or drug release devices, where uniform time steps can yield more accurate estimates (Figs. 3 and 6).
- *Improved Convergence and Stability with Adaptive Step Size:* The adaptive step-size approach significantly improves accuracy and rate of convergence with different tolerance values ($\in = 10^{-2}$, 10^{-4} and 10^{-5}), demonstrating the method's robustness for solving fractional IVPs (see Tables 6-9, 16-18 and Figs. 4-5, 7-8). In simulating biological processes, signal processing, and control systems—where abrupt changes in system dynamics require high resolution at particular times—this flexibility is extremely beneficial.
- *Computational Efficiency:* The novel approach achieves higher accuracy with lower computational cost to higher-order schemes, using less CPU time and enhancing efficiency, as shown in Tables 10 and 19. The effectiveness of this method makes the scheme suitable for real-time simulations in engineering domains such as vibration analysis of viscoelastic materials, fluid flow in porous media, and electrical circuits.
- *Applicability to Practical Problems:* The methodology serves as a powerful tool for dealing with physical challenges involving fractional dynamics in domains such as engineering, physics, and biology, where integer-order methods often fall short.

The fractional schemes described in this study will be extended in future studies to multi-term, stochastic, and coupled fractional models for more extensive real-world problems. The adoption of adaptive, parallel, and GPU-based algorithms will enhance precision and processing performance for complex nonlinear problems.

Conclusion

In this study, we created a novel numerical approach of fractional order employing the Caputo fractional derivative to solve FODEs. The local truncation error of the approach is $O\left(\frac{h^{3\vartheta}}{\Gamma(3\vartheta+1)}\right)$ with consistent order 2ϑ, according to the convergence study. The stability study reveals that $\text{FEM}_1^{[**]}$ has a large stability region and stability interval, as illustrated in Table 1 and Figs. 1 and 2. To verify the theoretical convergence study, certain numerical examples are considered. The numerical analysis is performed using a fixed step length and an adaptive step size strategy. The numerical results for fixed step length (Tables 2-6, 10-15) and an adaptive step size strategy (Tables 7-9, 16-19) clearly show that in terms of different error norms and CPU time, our method $\text{FEM}_1^{[**]}$ performs better and is a good alternative for solving linear and nonlinear fractional order differential equations compared to $\text{FEM}_1^{[*]} - \text{FEM}_3^{[*]}$. Our new developed technique has significantly higher computational efficiency than existing high-performance algorithms $\text{FFDM}^{[*]}$, $\text{FDDM}^{[*]}$ and $\text{FCSM}^{[*]}$, as illustrated in Tables 10 and 19. This emphasizes the importance of the established schemes in tackling the problems of solving fractional differential equations and confirms their superiority as reliable and efficient tools for solving FOIVPs in a variety of applications.

Future research will extend the proposed fractional-order schemes to higher-order methods, adaptive step-size strategies, and machine learning techniques for solving multi-term fractional differential equations. Large-scale systems, stochastic equations, and FOIVPs can all be solved using the techniques, which have parallel and GPU-based implementations. Comparative studies with deep learning-based solvers and real-world applications will help to confirm their performance and efficiency.

Data availability

The data that support the findings of this study are included within this article.

Received: 4 January 2025; Accepted: 24 March 2025

Published online: 15 April 2025

References

1. Mezic, I. & Banaszuk, A. Comparison of systems with complex behavior. *Physica D: Nonlinear Phenomena* **197**(1–2), 101–133 (2004).
2. Weber, J. & Wilhelm, T. The benefit of computational modelling in physics teaching: a historical overview. *European Journal of Physics* **41**(3), 034003 (2020).
3. Niu, W. C., Lin, J. C., Ju, Y. L. & Fu, Y. Z. The daily evaporation rate test and conversion method for a new independent type B LNG mock-up tank. *Cryogenics* **111**, 103168 (2020).
4. Van de Vosse, F. N. & Stergiopulos, N. Pulse wave propagation in the arterial tree. *Annual Review of Fluid Mechanics* **43**(1), 467–499 (2011).
5. Kleinstreuer, C. *Modern fluid dynamics* (CRC Press, Boca Raton, FL, USA, 2018).
6. Schulz, M. Control theory in physics and other fields of science: concepts, tools, and applications (Vol. 215). Springer Science and Business Media. (2006).
7. Magin, R.L. Fractional calculus in bioengineering: A tool to model complex dynamics. In Proceedings of the 13th International Carpathian Control Conference (ICCC) (pp. 464-469). IEEE. (2012, May).
8. Farhan, M. et al. A fractional modeling approach to a new Hepatitis B model in light of asymptomatic carriers, vaccination and treatment. *Scientific African* **24**, e02127 (2024).
9. Tang, T. Q. et al. A fractional perspective on the transmission dynamics of a parasitic infection, considering the impact of both strong and weak immunity. *Plos one* **19**(4), e0297967 (2024).
10. Shutaywi, M., Shah, Z. & Jan, R. A robust study of the dynamics of tumor–immune interaction for public health via fractional framework. The European Physical Journal Special Topics, 1-20. (2024).
11. Focardi, S.M. & Fabozzi, F.J. The mathematics of financial modeling and investment management (Vol. 138). John Wiley Sons. (2004).
12. Diethelm, K. & Ford, N. J. Analysis of fractional differential equations. *Journal of Mathematical Analysis and Applications* **265**(2), 229–248 (2002).
13. Davies, B. & Martin, B. Numerical inversion of the Laplace transform: a survey and comparison of methods. *Journal of computational physics* **33**(1), 1–32 (1979).
14. Shah, Z., Kumam, P. & Alreshidi, N. A. A meshless method based on the Laplace transform for the 2D multi-term time fractional partial integro-differential equation. *Mathematics* **8**(11), 1972 (2020).
15. Li, M.F., Ren, J.R. & Zhu, T. Series expansion in fractional calculus and fractional differential equations. (2009). arXiv preprint arXiv:0910.4819.
16. Khodadadi, E. & Karabacak, M. Solving fuzzy fractional Riccati differential equations by the variational iteration method. *International Journal of Engineering and Applied Sciences* **2**(11), 257796 (2015).
17. Askari, S., Allahviranloo, T. & Abbasbandy, S. Solving fuzzy fractional differential equations by adomian decomposition method used in optimal control theory. *International Transaction Journal of Engineering, Management, & Applied Sciences & Technologies* **10**(12), 1–10 (2019).
18. Jameel, A. F. et al. Solving first order nonlinear fuzzy differential equations using optimal homotopy asymptotic method. *International Journal of Pure and Applied Mathematics* **118**(1), 49–64 (2018).
19. Panahi, A. Approximate solution of fuzzy fractional differential equations. *International Journal of Industrial Mathematics* **9**(2), 111–118 (2017).
20. Diethelm, K. An algorithm for the numerical solution of differential equations of fractional order. *Electron. Trans. Numer. Anal* **5**(1), 1–6 (1997).
21. Odibat, Z. M. & Momani, S. An algorithm for the numerical solution of differential equations of fractional order. *Journal of applied mathematics & informatics* **26**(1_2), 15–27 (2008).
22. Biala, T. A. & Jator, S. N. Block implicit Adams methods for fractional differential equations. *Chaos, Solitons & Fractals* **81**, 365–377 (2015).
23. Pandey, R.K., Tiwari, N. & Singh, H. An Efficient Numerical Algorithm for Fractional Differential Equations. In Handbook of Fractional Calculus for Engineering and Science (pp. 151-168). Chapman and Hall/CRC. (2022).
24. Jator, S. N. & Coleman, N. A nonlinear second derivative method with a variable step-size based on continued fractions for singular initial value problems. *Cogent Mathematics* **4**(1), 1335498 (2017).
25. Batiha, I. M. et al. A numerical scheme for dealing with fractional initial value problem. *Int. J. Innov. Comput. Inf. Control* **19**, 763–774 (2023).
26. Batiha, I. M., Abubaker, A. A., Jebril, I. H., Al-Shaikh, S. B. & Matarneh, K. New algorithms for dealing with fractional initial value problems. *Axioms* **12**(5), 488 (2023).
27. Batiha, Iqbal M. et al. Modified three-point fractional formulas with Richardson extrapolation. *Mathematics* **10**(19), 3489 (2022).
28. Batiha, I. M. et al. A numerical scheme for dealing with fractional initial value problem. *Int. J. Innov. Comput. Inf. Control* **19**, 763–774 (2023).
29. Paul, S. K., Mishra, L. N., Mishra, V. N. & Baleanu, D. An effective method for solving nonlinear integral equations involving the Riemann-Liouville fractional operator. *AIMS Mathematics* **8**(8), 17448–17469 (2023).
30. Zureigat, H., Al-Smadi, M., Al-Khateeb, A., Al-Omari, S. & Alhazmi, S. E. Fourth-order numerical solutions for a fuzzy time-fractional convection-diffusion equation under Caputo generalized hukuhara derivative. *Fractal and Fractional* **7**(1), 47 (2022).
31. GuzmÃ¡n, F.S. Numerical Methods for Initial Value Problems in Physics. Springer. (2023).
32. Odibat, Z. M. & Momani, S. An algorithm for the numerical solution of differential equations of fractional order. *J. Appl. Math. Inform.* **26**, 15–27 (2008).
33. Sowa, M. Numerical computations of the fractional derivative in IVPS, examples in MATLAB and Mathematica. *Informatyka, Automatyka, Pomiary w Gospodarce i Ochronie Åšrodowiska* **7**(3), 19–22 (2017).
34. Workie, A.H. Small modification on modified Euler method for solving initial value problems. In Abstract and Applied Analysis (Vol. 2021, No. 1, p. 9951815). Hindawi. (2021).
35. Workie, A. H. New modification on Heunâs method based on contraharmonic mean for solving initial value problems with high efficiency. *Journal of Mathematics* **2020**(1), 6650855 (2020).
36. Batiha, I. M., Abubaker, A. A., Jebril, I. H., Al-Shaikh, S. B. & Matarneh, K. New algorithms for dealing with fractional initial value problems. *Axioms* **12**(5), 488 (2023).
37. Corless, R. M., Kaya, C. Y. & Moir, R. H. Optimal residuals and the Dahlquist test problem. *Numerical Algorithms* **81**, 1253–1274 (2019).
38. Dahlquist, G. On summation formulas due to Plana, Lindel öf and Abel, and related Gauss-Christoffel rules, I. *BIT Numerical Mathematics* **37**, 256–295 (1997).
39. Shams, M., Kausar, N., Ozbilge, E. & Bulut, A. Stable Computer Method for Solving Initial Value Problems with Engineering Applications. Computer Systems Science and Engineering, 45(3). (2023).
40. Diethelm, K., Ford, N. J. & Freed, A. D. A Predictor-Corrector Approach for the Numerical Solution of Fractional Differential Equations. *Nonlinear Dynamics* **29**, 3–22 (2004).

41. Bai, Z., Feng, L. & Hu, J. A Domain Decomposition Method for Time-Space Fractional Partial Differential Equations. *Applied Numerical Mathematics* **165**, 53–68 (2021).
42. Zayernouri, M. & Karniadakis, G. E. Fractional Spectral Collocation Methods for Linear and Nonlinear Fractional Differential Equations. *Journal of Computational Physics* **252**, 495–517 (2013).
43. Zabidi, N. A., Abdul Majid, Z., Kilicman, A. & Rabiei, F. Numerical solutions of fractional differential equations by using fractional explicit Adams method. *Mathematics* **8**(10), 1675 (2020).
44. Ford, N. J. & Simpson, A. C. The numerical solution of fractional differential equations: speed versus accuracy. *Numerical Algorithms* **26**, 333–346 (2001).

Acknowledgements
The authors express their sincere gratitude to the editor and reviewers for their insightful and constructive suggestions on the manuscript.

Declarations

Competing interests
The authors declare no competing interests.

Additional information
Correspondence and requests for materials should be addressed to A.A.

Reprints and permissions information is available at www.nature.com/reprints.

Publisher's note Springer Nature remains neutral with regard to jurisdictional claims in published maps and institutional affiliations.